Articles in PresS. J Neurophysiol (August 31, 2016). doi:10.1152/jn.01129.2015

Title

Robust modulation of arousal regulation, performance and frontostriatal activity through central thalamic deep brain stimulation in healthy non-human primates.

Authors

Jonathan L. Baker[1], Jae-Wook Ryou[1], Xuefeng F. Wei[2], Christopher R. Butson[3], Nicholas D. Schiff[1], Keith P. Purpura[1].

Affiliations

[1]Feil Family Brain and Mind Research Institute, Weill Cornell Medicine, New York, NY 10021.

[2]College of New Jersey, Department of Biomedical Engineering, Ewing Township, NJ 08618.

[3]University of Utah, Scientific Computing & Imaging (SCI) Institute, Department of Bioengineering, Salt Lake City, UT, 84112.

Running Head

Central thalamic stimulation robustly modulates performance

Address for Correspondence

Jonathan L. Baker PhD

job2037@med.cornell.edu

Feil Family Brain and Mind Research Institute

Weill Cornell Medicine, LC809

1300 York Avenue, New York, NY 10065

(212) 746-7669 (Office)

(212) 746-8050 (Fax)

Abstract

The central thalamus (CT) is a key component of the brain-wide network underlying arousal regulation and sensory-motor integration during wakefulness in the mammalian brain. Dysfunction of the CT, typically a result of severe brain injury (SBI), leads to long-lasting impairments in arousal regulation and subsequent deficits in cognition. Central thalamic deep brain stimulation (CT-DBS) is proposed as a therapy to reestablish and maintain arousal

regulation to improve cognition in select SBI patients. However a mechanistic understanding of CT-DBS and an optimal method of implementing this promising therapy are unknown. Here we demonstrate in two healthy non-human primates (NHP), *Macaca mulatta*, that location specific CT-DBS improves performance in visuomotor tasks and is associated with physiological effects consistent with enhancement of endogenous arousal. Specifically, CT-DBS within the lateral wing of the central lateral nucleus and the surrounding medial dorsal thalamic tegmental tract (DTTm) produces a rapid and robust modulation of performance and arousal, as measured by neuronal activity in the frontal cortex and striatum. Notably, the most robust and reliable behavioral and physiological responses resulted when we implemented a novel method of CT-DBS that orients and shapes the electric field within the DTTm using spatially separated DBS leads. Collectively, our results demonstrate that selective activation within the DTTm of the CT robustly regulates endogenous arousal and enhances cognitive performance in the intact NHP; these findings provide insights into the mechanism of CT-DBS and further support the development of CT-DBS as a therapy for reestablishing arousal regulation to support cognition in SBI patients.

New & Noteworthy

Severe brain injuries (SBI) annually encumber an estimated 125,000 individuals in the US with life-long cognitive disabilities and no effective therapies exist. Central thalamic deep brain stimulation (CT-DBS) is proposed as an effective therapy to reestablish arousal regulation to support cognition and here we demonstrate that CT-DBS robustly modulates cognition when stimulating a specific central thalamic target using a novel method. These results support our ongoing clinical studies to provide effective therapies for SBI patients.

Keywords

Central Thalamus, Deep Brain Stimulation, Arousal Regulation, Intralaminar Nuclei, Severe Brain Injury

Introduction

The central thalamus (CT) has long been considered an essential component of a larger arousal regulation network within the mammalian brain that maintains wakefulness and organizes resources in the anterior forebrain to support cognition and goal-directed behaviors (Schiff 2008; Mair et al. 2010). Humans with damage to the CT, as a result of severe brain injuries (SBI) of varying etiologies (Castaigne et al. 1981; Stuss et al. 1989, 1994; Adams et al.

2000; Van Der Werf et al. 2000, 2003; Maxwell et al. 2006; Little et al. 2010), persistently suffer from a variety of long-lasting cognitive impairments, including deficits in attention, episodic and working memory, information-processing speed, arousal regulation, executive functions (such as planning, initiating and directing actions, monitoring actions, problem solving, and inhibitory control), which significantly impact daily activities and their quality of life. (Dikmen et al. 2003; 2009; Levine et al. 2005; Ziino and Ponsford 2006; Ponsford 2013; Corrigan et al., 2014). These cognitive deficits lack robust therapeutic options (Talsky et al. 2010; Fridman and Schiff 2014) and deep brain stimulation within the central thalamus (CT-DBS) has been proposed (Schiff and Purpura 2002; Schiff 2012) as a therapeutic method for restoring arousal regulation and frontal-striatal-thalamic integration in SBI patients to facilitate and support rehabilitation. It fact, it has been demonstrated that CT-DBS can effectively restored multiple behavioral capacities, including functional recovery of speech and partial recovery of executive functions in an SBI patient who had remained in the minimally conscious state for over six years (Schiff et al. 2007).

Few studies, however have examined the basic mechanisms underlying CT-DBS and a precise clinical target for DBS in the central thalamus is unknown (Schiff 2012). To date, the rodent model has provided the best evidence supporting the use of CT-DBS for modulating arousal and global brain activity and studies conducted in intact rodents have demonstrated that modulation of innate or trained behaviors (Shirvalkar et al. 2006; Mair and Hembrook 2008) and shifts in arousal (Quinkert and Pfaff 2012; Gummadavelli et al. 2015) can be achieved with CT-DBS. In addition, recent studies have demonstrated that CT-DBS increases arousal and motor activity following repeated incidences of traumatic brain injury (TBI) in mice (Tabansky et al. 2014) and there exists a frequency dependence in the recruitment of frontostriatal populations during selective optogenetic activation of central lateral (CL) neurons (opto-CT-DBS) in the rat (Liu et al., 2015). While these rodent studies provide important data and insight, the future development of a human CT-DBS therapy necessitates a more precise characterization of CT-DBS in the larger brain of the intact NHP. NHPs are a well-established DBS research animal model that is closely linked phylogenetically with humans, share a prominent expansion of the anterior forebrain, and demonstrate the capacity to work over extended periods of time while performing complex goal-directed behaviors requiring sustained attention, working memory, speed, accuracy and motivation, all aspects of cognition not well characterized in rodent models.

Therefore in this study, for the first time, behavioral and physiological effects of CT-DBS were systematically explored in two healthy NHPs using custom designed CT-DBS systems scaled for the NHP and employing large-scale recording devices to broadly sample neuronal

activity from frontal and striatal areas of the anterior forebrain. The animals were trained to perform several visuomotor vigilance tasks, similar to tasks used to study vigilance or sustained mental effort in humans (Posner 1978; Davies and Parasuraman 1982; Luce 1984; Kinomura et al. 1996; Steinborn and Langner 2012), and when repeated over long time periods, produce significant demands on attentional resources. Performance variations and/or decrements on vigilance tasks in humans are attributed to fluctuations in arousal, motivation, distraction and boredom (Davies and Parasuraman 1982; Sarter et al. 2006; Langner et al. 2010) which can naturally lead to 'cognitive fatigue', a sequelae persistently experienced by many SBI patients (Dikmen et al. 2003; 2009; Levine et al. 2005; Ziino and Ponsford 2006; Ponsford 2013).

We show here that CT-DBS in the intact NHP facilitates behavioral performance and link these changes to endogenous arousal, as measured in the power spectra of local field potential (LFP) activity recorded within frontal and striatal cell populations of the anterior forebrain. Critically, we discovered that a maximal behavioral and physiological effect is achieved when the electric field is shaped and elongated within a specific region of the CT through the use of adjacent pairs of DBS leads separated by several millimeters along the anterior-posterior axis, here termed 'field-shaping CT-DBS'. In this study, the impact of CT-DBS on behavioral performance and frontostriatal activity as demonstrated in intact NHPs is aimed at translating these novel results into new therapeutic options for persons suffering from the chronic cognitive sequelae following SBI (Schiff 2012).

Methods

Study design

All work was performed in strict done in accordance with the National Institutes of Health Guidelines for Use of Animals in Research and under an approved protocol from the Weill Cornell Medical College Institutional Animal Care and Use Committee (IACUC). A detailed description of the surgical techniques, behavioral control and data acquisition systems can be found elsewhere (Purpura et al. 2003; Schiff et al. 2013).

In this study, behavioral and physiological data were collected over a 30-month period in NHP1 and over an 18-month period in NHP2. Experimental sessions were conducted in a block design, where each animal was provided several 2, 4 and/or 6-month breaks between blocks of experimental sessions to maintain their health and to facilitate data management and analysis. The animals were euthanized to reconstruct all recording and stimulation sites once an adequate amount of behavioral and physiological data were collected. For this study, 218 experimental sessions in NHP1 and 68 in NHP2 were analyzed. In NHP2, 234 DBS periods

were excluded because stimulation was conducted within the fasciculus retroflexus, (i.e. habenula-peduncular tract), a robust bundle of fibers that traverse the center of the Pf nucleus, a component of the caudal central thalamus (Sutherland 1982; Jones 2007), and results from fasciculus retroflexus DBS (fr-DBS) are not the focus in this study. Numerous CT-DBS experimental sessions in both animals were excluded if the animals' starting performance was low (<20%) or they refused to work for water rewards. These sessions are presumed to reflect days of low motivation as a result of factors beyond the control of the investigators related to facility operations, group housing, and animal care. Additional experimental sessions, including electroanatomy and behavioral data were collected during the monopolar, bipolar and multipolar field-shaping reviews of the DBS contacts in both animals but are not included in this study.

Behavioral experiments

Here we modeled 'cognitive fatigue' using simple vigilance tasks that produce significant demands on cognitive resources in the intact NHP by requiring sustained 'mental effort' (Sarter et al. 2006) over extended periods of time. Performance decrements in these tasks are identified as an increased rate of incorrect and/or incomplete trial performance accompanied by a slowing and increased variance of reaction times, and a greater prevalence of eye closure, drowsiness and putative 'sleep' episodes near the latter half of experimental sessions (Fig. 1*B,C*; Smith et al. 2009; Shah et al. 2009). Motivation influences performance throughout the tasks, however this aspect of performance was not systematically investigated, as has been done in other NHP studies (Bouret and Richmond 2015; Varazzani et al., 2015). Additional experimental sessions were conducted where reward schedule was randomized or significantly decreased and/or increased over blocks of trials to assess motivation, however these data are not included in this study. We found that the animals continued to monitor reward value prior to, during and after CT-DBS (data not shown) throughout a day's experimental session and would predictably shift performance depending on reward size, as demonstrated in other NHP studies (Bouret and Richmond 2015; Varazzani et al., 2015).

Behavioral experiments were programmed and implemented using a real-time computer control system (TEMPO, Reflective Computing, St. Louis, MO, running under DOS 6.0; Microsoft, Redmond, WA). The video display monitor (SONY) was controlled by a VSG2/3 graphic processor (Cambridge Research Systems, Kent, UK) with a refresh rate of 100Hz and positioned 114cm from the bridge of the nose of the head fixed animals. Control signals between the TEMPO and VSG2/3 computers used standard DIO protocols. Eye position was measured and tracked using horizontal and vertical analog voltage signals from an E5000

infrared video eye tracking system fitted with a telephoto lens (ASL, Bedford, MA). The animal's gaze position was calibrated each day prior to experiment sessions and then modified whenever necessary to ensure the accuracy of the calibration. Horizontal and vertical eye position signals were recorded and processed to determine the occurrence of saccades, their amplitude, velocity, direction, and the positions and durations of fixation periods. Fixation during the task was considered to be broken if the eye position left a 2.5–3.5° window around the fixation targets. The eye tracker has a resolution of 1.3° of visual angle.

The animals performed a modification of a standard variable delay period reaction time task "S1–S2," or "phasic alerting" paradigm used in humans and in prior NHP studies (Posner 1978; Kinomura et al. 1996; Smith et al. 2009; Shah et al. 2009; Schiff et al. 2013). Briefly, the structure of this task is initiated by the appearance of a target (a black/red checkerboard or dartboard 5 degree x 5 degree of visual angle) at one of 9 locations (chosen at random on each trial) on a CRT monitor positioned in front of the animal. After a 1 second period of stable fixation of the target, the target underwent contrast reversal at 10 Hz for a variable delay period until changing to a black/green checkerboard or dartboard (Fig. 1*A*). The transition to black/green from black/red was the 'GO' signal for contacting the infrared touch switch located within the primate chair (Crist Instrument Co. Inc., Hagerstown, MD). The variable delay period was randomly drawn from a normal distribution with mean of 2500ms and standard deviation of 250ms. A trial was considered to be incorrect if the NHP broke fixation prior to the 'GO' cue or touched the IR switch before or within 250ms after the 'GO' cue (early touch) or failed to respond within 800ms after the green target (late touch).

In addition to the vigilance task, NHP1 was trained to perform a memory guided saccade task (Hikosaka and Wurtz 1983). Briefly, the animal was required to fixate a central green fixation square for 500ms and a white square ('target') would briefly appear (80ms) randomly in 1 of 8 positions located in the periphery, each equidistant from the central fixation square. The animal was required to maintain fixation for a variable delay period randomly drawn from a normal distribution with mean of 2500ms and standard deviation of 250ms, until the central fixation spot extinguished. The animal then had to make a saccade to the remembered location of the target. If the saccade was performed correctly, the target reappeared 300ms after the end of saccade and the NHP was only rewarded if fixation was held at the target position for 500ms. A trial was considered to be incorrect if the NHP broke fixation or the saccade to the target was not within a 2.5 to 3.5 degree window within 500ms of the fixation spot offset.

Electrophysiological recording methods

Following successful behavioral training, the two adult male NHPs (*Macaca mulatta*), NHP1 (11kg) and NHP2 (10kg) were imaged using standard high resolution MR and CT series to construct a surgical plan for targeting the central thalami with DBS leads and frontal and striatal locations with microelectrodes. Several recording chambers (Gray Matter Research, Bozeman, MT) and a head fixation post (Crist Instruments Co. Inc., MD) were then implanted using standard sterile surgical technique under deep Isoflurane anesthesia (as described in detail in Purpura et al. 2003). A high-density 32-microelectrode microdrive (Model SC32, Gray Matter Research LLC, Bozeman, MT) was positioned over the right frontal cortex of both animals to chronically record broadband signals from frontal eye fields (FEF), dorsal lateral prefrontal (DLPF), dorsal premotor (PMd) and dorsal caudate and putamen. Each microelectrode (Alpha Omega LTD, Nazareth, Israel) was attached to a lead-screw and shuttle and had a maximum linear travel depth of ~20mm. The ~6 x 6 electrode grid spanned 7.5mm with an inter-electrode spacing of 1.5mm. To isolate unit activity, the position of each microelectrode was adjusted prior to each recording session with a custom screwdriver (1 rotation ~125um) and precise recording depths were cataloged and adjusted relative to the cortical surface following the histology. Gray to white matter boundaries during the experiments were judged based on recording depth, lack of unit activity, and high impedance characteristics of white matter and were used to exclude LFP recordings from microelectrodes presumed to be outside of gray matter. In NHP1 3295 independent microelectrode recording sites and 206 in NHP2 were included in this study. The lower number collected in NHP2 resulted from a mechanical disruption of the microdrive requiring its early removal and cessation of microelectrode recordings from the frontal cortex. In addition to the microdrives, custom 10-channel ECoG arrays were chronically implanted to record from the animal's cerebral cortices. The ECoG arrays consisted of radiotranslucent 4mm Ag-AgCl electrodes (BioPac Systems Inc., Goleta, CA) bonded to 2x6mm titanium bone screws (Salvin Dental Specialties, Charlotte, NC) that penetrated the skull and touched the dural surface.

All neurophysiological signals were recorded with the RZ2 data acquisition system (Tucker Davis Technologies, Alachua, FL) at a maximum rate of ~25KHz. Task relevant signals, horizontal and vertical eye signals (High speed stationary Optics, ASL, Bedford, MA) were synchronized and recorded with the RZ2 system. For all DBS experimental sessions, high-resolution video (Panasonic HDC-HS900K, 1080p at 30fps) of the animals performing the tasks was synchronized with the data acquisition system and stimulator.

Central thalamic deep brain stimulation rationale and methods

239 We chronically implanted multiple DBS leads scaled for the NHP (Elder et al. 2005),
240 based on human DBS leads (Model 3387, Medtronic, Minneapolis, MN), into the thalami of two
241 NHPs to systematically stimulate multiple CT targets using various standard and novel
242 configurations of DBS. Intralaminar thalamic neurons of the CT send diffuse projections to large
243 expanses of cortex and striatum (Macchi and Bentivoglio 1986; Jones 2007) and exhibit unique
244 firing properties (Glen and Steriade 1982; Steriade et al. 1993) that shift markedly during
245 periods of arousal. Cellular groups of the CT that represent promising DBS targets for restoring
246 arousal regulation in SBI humans (Schiff 2008) include the rostral central lateral (CL), the
247 paracentral (PC) nuclei, and the caudal centromedian-parafascicular complex (CM-Pf), which
248 are all accessible to DBS lead penetrations through the overlying somatosensory and parietal
249 cortices. Modulations in the firing rates of these neuronal populations are linked to cognitive
250 function and grade with task performance in NHPs (Schlag and Schlag-Rey 1971, 1984;
251 Schlag-Rey and Schlag 1984; Matsumoto et al. 2001; Wyder et al. 2003, 2004; Minamimoto et
252 al. 2009; Schiff et al. 2013). These same regions exhibit graded activation in humans performing
253 similar visual attention tasks (Kinomura et al. 1996; Paus et al. 1997; Portas et al. 1998) hence
254 their proposed role in arousal regulation (Schiff and Purpura, 2002; Schiff 2008) and as potential
255 DBS targets in select SBI patients (Schiff 2012).

256 DBS is known to produce a mixture of effects in neural tissue (McIntyre et al. 2004; Vitek
257 et al. 2008; Montgomery and Gale 2008). Therefore we used a DBS waveform that mirrors the
258 output of the Medtronic Inc. clinical system (as described in Butson et al., 2011), which is
259 designed to safely and optimally stimulate large myelinated axons (Nowak and Bullier 1998;
260 Merrill et al. 2005). The DBS waveform consisted of an 80μs square cathodal pulse followed by
261 an isoelectric period of 60μs and ended with a 400μs square anodal pulse to balance the total
262 charge injected. Each pulse lasted a total of 540us. During the experimental sessions
263 stimulation was delivered in standard monopolar, bipolar and novel multipolar, field-shaping
264 configurations, at various frequencies (20, 40, 150, 175, 200 and 225Hz) and amplitudes (0.25-
265 3.0mA) under current control, in order to maintain pulse shape over time-varying impedances
266 for each contact (Lempka et al. 2010). In this study, periodic DBS was used to activate
267 (Hashimoto et al. 2003; Garcia et al. 2003, 2005) CT cellular populations and the DTTm (Edlow
268 et al., 2012), which is composed of thalamic efferents and en passant fibers within the internal
269 medullary lamina that encase the CT nuclei (Macchi and Bentivoglio 1986; Jones 2007). Our
270 goal was to artificially enhance the afferent drive into various anterior forebrain targets (Macchi
271 and Bentivoglio 1986; Steriade 2000; Minamimoto and Kimura 2002; Jones 2007) thereby

'activating' the anterior forebrain (Steriade et al, 1991; Steriade 2000) to robustly modulate behavioral performance.

Based on the successful demonstration of behavioral facilitation utilizing bilateral monopolar and bipolar CT-DBS in a single SBI subject (Schiff et al. 2007), we conducted a review of standard *intra-lead* monopolar and bipolar stimulation configurations of all viable contacts to thoroughly evaluate behavioral and physiological effects was performed in both animals. The reviews consisted of a linear 0.25mA ramp of current, from 0.25 to 3.0mA, using 150Hz stimulation frequency. Behavioral responses, including eye, pinnae and body movements, vocalizations and generalized changes in normal activity in the form of hyperkinetic movements, abrupt shifts in posture or localized touching suggestive of paresthesias were noted. Consistent behavioral responses during these reviews were noted and the current level for each termed 'threshold'. The monopolar configurations used the titanium bone screws and titanium bone plate located within the diploë of the occipital calvarium for current return. The standard *intra-lead* bipolar configurations placed anode(s) and cathode(s) contacts on the same DBS lead. We suspended use of monopolar CT-DBS during the experimental sessions due a combination of electrical artifact issues and nonspecific motor, visuomotor and somatosensory effects produced in the first animal that consistently interrupted task performance at lower than anticipated current levels. Standard bipolar CT-DBS with one or two leads was then pursued more systematically and during this process we discovered that *inter-lead* bipolar CT-DBS (where anode(s) and cathode(s) are placed separately on the contacts of the two spatially separated DBS leads), here termed field-shaping CT-DBS (fsCT-DBS), was more effective in facilitating behavioral performance and frontostriatal activity in both animals. Here, fsCT-DBS is produced by any configuration that assigns the anode(s) and cathode(s) to separate DBS leads displaced by several millimeters within the central thalamus.

Custom deep brain recording and stimulation (DBRS) devices with a 13-position radial grid were developed to guide multiple DBS leads (0.75mm OD) into the thalami. Each DBS lead has six platinum/iridium annular contacts (impedances 1.0-10kΩ), each 0.5mm in height, with an intra-lead spacing of 0.5mm and insulated by polyurethane (NuMED, Inc., Hopkins, NY). A maximum current density of 2.6mA/mm^2 and maximum charge density of 20.4uC/cm^2/phase was delivered during 3.0mA stimulation during this study. The surface of each contact was coated with BT DOT (Biotectix, Ann Arbor, MI) prior to implantation to reduce and stabilize the impedance levels of each contact. Impedance levels were measured on a weekly basis with a metal electrode impedance tester model IMP-1 (Bak Electronics Inc., Sanford, FL) using a 1KHz signal. Contacts with impedances above 10KΩ were not used in order to limit waveform

distortions delivered to the tissue. Waveforms were passed through a custom-built current sensing circuit and visualized on a digital oscilloscope (TBS1000, Tektronix, Inc. Beaverton, Oregon) to confirm the presence and/or absence of waveform distortions. From the distal contact of the DBS lead, individual contacts were numbered 0 to 5. The free ends of the DBS contacts were connected to a low profile 6-pin Nano Circular Connector (Omnetics Connector Corp. Minneapolis, MN) and rigidly secured within the DBRS system.

In NHP1, two DBS leads were implanted into the right thalamus with an inter-lead separation of 2.4mm. In NHP2, two DBS leads were implanted into the right thalamus with an inter-lead separation of 1.8mm and two DBS leads were implanted into the left thalamus with an inter-lead separation of 2.7mm. In NHP1 DBS lead locations and inter-lead spacing were set to optimize targeting of the 'wing' of the central lateral (CL) nucleus (Glen and Steriade 1982), principle CT fibers and en passant fibers (Scheibel and Scheibel 1967; Jones 2007) of the DTTm based on post-operative reconstruction of fiducial guidetube markers relative to the modeled CT nuclei (Paxinos et al. 1999). We estimated a spatial uncertainty of about 1mm or less in electrode positions based on the MR image resolution and histological confirmation of the DBS lead locations. Based on preliminary behavioral and physiological results obtained in NHP1, DBS leads in NHP2 were positioned to target the caudal CM-Pf component of the CT and more medial portions of medial dorsalis (MD). Model reconstruction of the DBS leads and individual contact locations relative to the CT targets are noted below in the modeling and results sections, respectively. Conformation of lead locations was determined through standard Myelin and nissl histology (FD Neurotechnologies, Inc. Colombia, MD), light microscopy and comparison with neuroanatomical atlases of the NHP (Paxinos et al. 1999, scalablebrainatlas.incf.org).

A four-channel Multi Channel Systems GmbH (MCS) stimulator (STG4004-3.2mA) with a compliance of 120 volts was connected to the DBS leads to deliver stimulation. Each of the four channels of the MCS stimulator is optically isolated to ensure reliable current delivery when multiple channels are used simultaneously. Timing of the MCS stimulator was controlled with TTL pulses generated by the TDT RZ2 system and synchronized with the behavioral control computer. All DBS pulse times and voltage waveforms were collected with a TDT RP2.1 Enhanced Real-Time Processor at a sampling rate ~100KHz to visual and identify waveform distortions.

Modeling DBS activation in the central thalamus

339 Computational models were used to predict the effects of DBS in each NHP. These
340 predictions have been validated in prior human and NHP studies (Butson et al, 2007; Miocinovic
341 et al, 2009), and methodological details can be found in previous publications (Butson et al,
342 2011; Butson and McIntyre 2008). Briefly, pre- and post-operative CT and MR imaging enabled
343 surgical planning and model reconstruction relative to the targeted central thalamic nuclei. The
344 computational model of CT-DBS consists of four main components: 1) an animal-specific 3D
345 anatomical model of major thalamic nuclei constructed from the Paxinos atlas ((Paxinos et al.
346 1999), scalablebrainatlas.incf.org) that was registered to each NHP's pre- and post-operative
347 CT and MR imaging data; 2) a finite element model of the 6-contact DBS leads and electric
348 fields generated in a physiological medium (Butson et al. 2007); 3) multi-compartmental 5.7μm
349 cable model neurons distributed around the leads and 4) probabilistic fiber orientations of
350 neurons based on a diffusion tensor (DTI) brain template for rhesus macaques (Adluru et al.
351 2012). The model served two main purposes: 1) to provide stereotaxic coordinates of the CT
352 nuclear targets to accurately guide the placement of multiple DBS leads; 2) to visualize the
353 predicted axon activation during DBS under the various stimulation parameters conducted in
354 this study.

355 A 3T Siemens MAGNETROM TRIO was used to collect high-resolution MR images
356 ($0.5mm^3$ voxel) with enhanced contrast (Ablavar, Lantheus Medical Imaging Inc., North
357 Bellerica, MA) and a General Electric Medical Systems Discovery LS Model was used to collect
358 CT images with a voxel depth of 1.25mm. Analyze 9.0 software (Mayo Clinic, Rochester MN)
359 was used to outline the individual thalamic nuclei across atlas slices, and SCIRun 4.5 software
360 (Scientific Computing & Imaging Institute, University of Utah, Salt Lake City, UT) was used to
361 co-register the 3D thalamic nuclei with all MR and CT imaging using a previously published
362 algorithm (Viola and Wells, 1997). Following the initial implantation surgery lead contact
363 locations were estimated through isosurface processing of post-operative CT images.

364 A finite element model (COMSOL 3.5) was created to estimate the electric field
365 produced during DBS. This model accounted for the encapsulation layer around the electrode
366 and in vivo impedance measurements (Butson et al. 2007). Extracellular potentials were applied
367 to multi-compartment cable models of myelinated axons (McIntyre et al. 2002) distributed
368 around the DBS leads and the diffusion tensor template of the NHP (Adluru et al. 2012) was
369 used to select axon directions and locations that met stimulation criterion set during the
370 behavioral experiments. Axon activation maps were generated as point clouds presenting the
371 nodes of action potential initiation that met stimulation threshold criterion. The same charge-
372 balanced asymmetrical biphasic square pulses used during the experiments were applied in the

model and the time-dependent transmembrane potentials induced by the stimulation pulses were calculated in NEURON 7.1 (Hines and Carnevale 1997).

Histology

Histology staining was performed by FD Neurotechnologies Inc. (Columbia, MD). Following standard transcardial perfusion, formaldehyde-fixed (4%) tissue blocks containing the tracts of the DBS leads were dehydrated through graded ethanol and xylenes, and then embedded in paraffin. Serial sections (10 μm in thickness) were cut through the whole tissue block with a rotary microtome. The 1st section of every group of 4 (or 10) sections following the discovery of the DBS lead tract was mounted on 25x75 mm Superfrost Plus microscope slides. All sections were stained with FD Luxol fast blue solution™ and counterstained with FD cresyl violet solution™ to mark mylienated fibers and cell bodies, respectively. Sections were cleared in xylene and then coverslipped in Permount (Fisher Scientific, Fair Lawn, NJ). Slides containing the DBS lead tracts were digitized with a microscope using a 2X objective and compared with a standard histology atlas of the NHP (Paxinos et al. 1999, scalablebrainatlas.incf.org) to identify thalamic nuclei and major fiber tracts. Cortical and striatal recording sites were identified from Nissl stained sections and electrode recording depths were adjusted based on the histology.

Behavioral data analysis

When motivated to work for liquid rewards the animals performance was typically high at the start of each experimental session and then gradually diminished as total time on task increased (Fig. 1*B,C*, Smith et al. 2009; Shah et al. 2009, Schiff et al. 2013). Correctly performed trials included reaction times relative to the ‘GO’ cue occurring between 250 and 800ms in the vigilance task and between 150 and 500ms in the memory guided saccade task. Incorrect trials are categorized as ‘incomplete’ trials (broken fixation, early and late touch of the IR switch) and ‘incorrect’ trials (failure to acquire the target, failure to respond after the ‘GO’ cue). The second type of ‘incorrect’ trial occurred rarely. An estimate of behavioral performance is computed from the time series of correct, ‘1’ and incomplete and/or incorrect, ‘0’ trials, using a state space modeling approach (Smith et al. 2009). This smooth estimate of performance rate was used to visualize performance as a function of trial number in relation to the CT-DBS ON and OFF periods (Fig. 1*B,C*, 2*A,C*).

The odds ratio was used to quantify the effect size of DBS relative to baseline performance by calculating the ratio of the odds of getting a correct trial during CT-DBS ON periods to the odds of getting a correct trial during CT-DBS OFF periods. Odds ratios for all

DBS periods were computed and subjected to a 95% confidence based on the standard error and the total number of trials in both the ON and OFF periods. A minimum of 20 trials prior to the onset and 20 trials during DBS were required for a DBS period to be included in this study. Reaction time distributions of correctly performed trials during ON and OFF DBS periods were compared using a ranksum test with a significance of $p<0.05$. The coefficient of variation (CV), the standard deviation divided by the mean reaction times, was used to quantify the variance of reaction times within a set period.

Electrophysiological data analysis

Broadband activity (0.1-10KHz) was collected from custom high impedance (0.5-1.5MΩ) microelectrodes (Alpha Omega LTD, Nazareth, Israel) positioned within a 32-microelectrode microdrive (SC32, Gray Matter Research LLC, Bozeman, MT). The power spectra of the LFP signals were calculated using the multitaper method (Mitra and Pesaran 1999; Thomson 2002; Mitra and Bokil, 2008) implemented in the Chronux toolbox (http://www.chronux.org) to control the bias and variance in the spectral estimates of neurophysiological signals using the mtspectrumc.m function. The log-transformed power spectra were subjected to a bias-corrected two-group test to adjust for the unequal sample sizes that often arise when comparing across treatment conditions (Bokil et al. 2007). At each frequency, the difference between the power spectra for the ON versus OFF DBS periods was divided by an estimate of the variance in the two-group sample (Bokil et al. 2007). In addition, the p-values of the resulting Z-scores across the power spectra were subjected to a false-discovery rate (FDR, $p<0.05$) test to correct for multiple comparisons arising from the multiple frequencies in the spectra (Benjamini and Hochberg 1995). Z-scores that passed screening of the two-group and FDR tests (two_group_test_spectrum.m) were used to construct a distribution at each frequency of significant power differences in the LFPs between DBS ON and OFF conditions. Z-score means and confidence intervals were computed by standard methods.

ECoG signals were recorded from a custom array of 10 electrodes distributed over frontal, temporal, parietal and occipital cortices. In this study, a bipolar montage of two midline ECoG electrodes, roughly corresponding to human Fz and Cz, was used to monitor activity throughout each experimental session in both animals. The power spectra of the Fz-Cz ECoG signal were calculated using the same multitaper routines as described above. A significant increase in the power spectra within the low frequency band (4-12Hz) was consistently correlated with eye-closure and putative ‘sleep’ episodes during the OFF DBS periods.

Electrical stimulation artifacts in neurophysiological signals

Stimulation artifacts were generated in all neurophysiological signals collected during CT-DBS when stimulation amplitudes of 0.5-3.0mA were used. The high-frequency nature of the DBS pulse affected the majority of microelectrode recordings and precluded the analysis of unit activity during DBS in this study. During monopolar stimulation, the preamplifier (PZ2-32, Tucker Davis Technologies, FL) was close to half saturation; therefore we did not analyze these data. However, during standard and field-shaping multipolar CT-DBS the artifact was well below the saturation point of the preamplifier that included a 4th order low-pass (24 dB per octave) at 7.5 kHz anti-aliasing filter for each channel and therefore did not impact the LFP through saturation or aliasing artifacts. All microelectrode broadband signals were recorded at ~25KHz and the ECoG signals were recorded at 1KHz. A digital Butterworth filter (filtfilt.m, 4th order, 3dB per octave) was used in custom Matlab software (Mathworks, Natick, MA) to remove the stimulation artifacts without distorting the power spectrum of the LFP signals (0.1 to 50Hz). We tested this assumption by randomly and periodically introducing a series of stimulation artifacts waveforms with varying amplitudes to actual non-DBS microelectrode broadband signals and then subjecting them to the above analysis. The high frequency components of the added DBS artifacts had 0dB impact on the power spectrum of the LFP signals (0.1 to 50Hz).

In addition to the digital signal processing methods described above, we followed standard industry protocols to test our recording electronics (TDT RZ2-DAQ) during high amplitude and high frequency DBS and for characterizing and removing stimulation artifacts from biological signals (Stanslaski et al. 2012 and personal correspondence with Dr. Timothy Denison at Medtronic Inc. Minnesota, MN). Briefly, the same Alpha-Omega microelectrodes (0.5 to 1.5MOhms) used to record broadband (0.1-8000Hz) neural activity in the animals were placed into a 300cc physiological saline bath and positioned 20mm from the active contacts of two spatially separated DBS leads in order to approximate the distance between the central thalamic stimulation locations and the frontal cortex and dorsal striatum of the animals. Tests were conducted using multiple separation distances between the microelectrodes and the two DBS leads, ranging from 1-50mm and 2-4mm respectively. Electric stimulation through the DBS leads was then introduced to the saline bath using the same standard and field-shaping stimulation protocols with 150, 175, 200 and 225Hz stimulation frequencies and amplitudes ranging from 0.25 to 3.0mA. In addition, sinusoidal test signals (10-50Hz) of various amplitudes were introduced into the saline bath using a separate copper wire connected to a function generator and the signals were recorded through the microelectrodes using the identical experimental setup, without the animal, to mimic the amplitude of the recorded LFP oscillations.

The same broadband recording, filtering and spectral analysis described above was conducted on the recorded signals containing the known sinusoidal test signals (10-50Hz). In conclusion we determined that all electric stimulation artifacts generated contributed 0dB change in all sinusoidal test signals (10-50Hz), for all DBS lead configurations, stimulation parameters and inter microelectrode-DBS lead separation distances. After conducting these standard industry protocols, we are confident that the measured changes in the frontostriatal LFP power spectra during all CT-DBS configurations conducted in this study are neurogenic in origin.

Results

Two adult NHPs *(Macaca mulatta)* were implanted with custom recording and DBS devices (*see Methods*) and trained to perform several visually guided motor reaction time tasks with variable delay periods for water rewards (Fig. 1*A*). In the absence of CT-DBS (Fig. 1B,C) behavioral performance of both animals was typically high at the start of an experimental session and then gradually decreased over time, as observed in other NHPs performing identical tasks (Smith et al. 2009; Shah et al. 2009; Schiff et al. 2013). Performance decrements included an increased rate of incorrect and/or incomplete trials, increased variance of reaction times, and a greater prevalence of eye closures and putative 'drowsiness' and 'sleep' episodes (as assessed through power fluctuations in midline Fz-Cz ECoG recordings, *see Methods*) near the latter half of the experimental sessions (Fig. 1*B,C*). This transition in behavioral performance is consistent with a shift from a state of a high arousal and motivation at the start of the session to a state, as time on task increases, of greater satiety, boredom, drowsiness and low motivation, vigilance and vigor (Sarter et al., 2006). Humans show similar changes in behavioral state when conducting similar long, sequential multi-trial tasks (Paus et al., 1997).

In the example non-DBS sessions shown in Figure 1*B,C*, the animals' performance begins to decline following trial 600, corresponding to 43 to 68 minutes time on task. Putative 'sleep' episodes (indicated with green markings along the zero performance line) are seen in both animals. Following trial 600, the CV of the reaction times increases slightly from 0.15 to 0.17 in NHP1 and in NHP2 reaction time CV increases markedly from 0.1 to 0.15, while average reaction times do not significantly change (ranksum, $p>0.05$). The animals remain on task for 80 and 120 minutes until satiated at which point they refused to work for additional water rewards. During CT-DBS experimental sessions, time on task ranged from 35 to 262 minutes for NHP1 and 35 to 227 minutes for NHP2. Shorter experimental sessions presumably reflected days of lower motivation. In NHP1, 218 experimental sessions with CT-DBS were recorded during 137

days and in NHP2, 68 experimental sessions with CT-DBS were recorded during 57 days (*see Methods*).

Behavioral performance is robustly modulated with central thalamic deep brain stimulation

Periodic high frequency fsCT-DBS, when conducted over blocks of contiguous trials and shown as colored regions in Fig. 2*A,* modulates robustly the animal's performance. In this example, only the first 1600 of 2500 trials are shown, even though robust modulation of performance was observed throughout the entire session. Behavioral performance is quantified using the odds ratio. The log of this ratio is the log odds ratio (LOR) and positive LOR values correspond to a greater probability of the animal performing a correct trial during the DBS period. Significance of the LOR value ($p<0.05$) is based on the number of trials in the DBS ON and OFF periods, which were roughly equal in number (*see Methods*).

In Fig. 2*A* each field-shaping CT-DBS (fsCT-DBS) period is colored gray or green to reflect the significance of the LOR value, with significantly positive periods indicated by green ($p<0.05$) and non-significant ($p>0.05$) by gray. During the initial 'induction' phase the majority of LOR values range from -2.1 to 0.7 ($p>0.05$) and are colored gray, except for the two periods colored green, corresponding to positive LOR values ($p<0.05$) that demonstrate a significant facilitation of performance during fsCT-DBS. During the 'control' phase, LOR values of the fsCT-DBS periods are all positive and significant, ranging from 3.8 to 6.7 ($p<0.05$) indicating robust facilitation of performance during fsCT-DBS. Operationally in this study, we use the terms 'induction' and 'control' to highlight the transition to an extended block of trials where ON and OFF periods of fsCT-DBS were more positively correlated with correct performance of the task. Of note, both animals did perform during the 'control' phase without fsCT-DBS; therefore performance was not exclusively contingent on fsCT-DBS, as seen in both animals (Fig. 2). Here 'control' represents a period during an experimental session where resumption of reliable performance from a low or near zero baseline is observed in a sequence of blocked trials and quantified using the LOR.

Time-dependent properties of fsCT-DBS behavioral performance

Modulation of behavioral performance by fsCT-DBS displays several time-dependent properties. First, the influence of fsCT-DBS on performance and reaction times develops over the experimental session. The initial periods of fsCT-DBS primarily affect reaction times, where median reaction times for ON fsCT-DBS periods (385 ms, 164 correct trials) are significantly shortened by 40 ms (ranksum, $p<0.05$) between trials 200 and 600 as compared with the

interleaving OFF periods (164 correct trials) (Fig. 2*B*). However, the reduction in reaction times did not persist and once 'control' is established after trial 700 median reaction times are slightly increased and more variable (CV of 0.16, compared to CV of 0.07), yet significantly different (ranksum $p<0.05$) for ON (400ms, 72 correct trials) and OFF (415ms, 554 correct trials) fsCT-DBS periods during the remainder of the session.

Second, the distinct behavioral profiles of 'induction' and 'control' phases observed in NHP1 (Fig. 2*B*), occurred in 153 out of 187 experimental sessions when fsCT-DBS was used, however the duration of the 'induction' phase varied across experimental sessions. In some the shift from 'induction' to 'control' was rapid, occurring within the first or second fsCT-DBS period (~20 minutes time on task), and for others, the shift occurred later, after several fsCT-DBS periods, (1-12 periods, median 2), as seen in Fig. 2*B* after the 8th fsCT-DBS period (first period that is colored green). Importantly, the 'control' phase observed in NHP1 was never achieved with standard CT-DBS configurations even though performance could be facilitated (Fig. 4*C*). Here, we postulate that the 'control' phase represents a state of performance recovery, whereby fsCT-DBS is able to boost performance back to levels achieved earlier in the experimental session. Of note, NHP1 did resume performance during the 'control' phase without fsCT-DBS when enough time had elapsed between periods of stimulation, as seen around trials 1140 and 1415 (Fig. 2*B*), demonstrating that the animal was still able to mobilize its own resources and resume performance. Spontaneous resumption of performance while in the 'control' phase and during OFF fsCT-DBS periods was observed in all 21 experimental sessions when time between fsCT-DBS ON periods was purposefully extended.

Comparable time-dependent effects in behavioral performance were observed in NHP2 when a similar high frequency fsCT-DBS protocol was used (example session shown in Fig. 2*D*). Here current levels between 0.5 and 1.0mA either facilitated (green periods) or had no effect (gray periods) on behavioral performance, while stimulation amplitudes above 1.0mA, colored in red, consistently suppressed performance (Fig. 2*D*). During the 'induction' phase in Fig. 2D, LOR values of fsCT-DBS periods are positive but not significant, ranging from 0.1 to 0.6 ($p>0.05$), when amplitudes are 0.5 to 1.0mA and significantly negative, ranging from -1.7 to -5.1 ($p<0.05$), when amplitudes above 1.0mA were used. During the 'control' phase, stimulation amplitudes between 0.75 and 1.0mA consistently facilitated performance (green periods) or had no effect (gray periods), while stimulation amplitudes above 1.0mA (red periods) continued to suppress performance (Fig. 2*D*). Overall, the shift from 'induction' and 'control' phases observed in NHP1 were not consistently observed in NHP2, however a resemblance of these 'phase' transitions, where increased performance correlated with fsCT-DBS in the latter half of the

experimental session, was observed in 20 out of 46 experimental sessions, occurring on average in the 5th or 6th fsCT-DBS period (range 1 to 12 fsCT-DBS periods), corresponding to ~50 minutes time on task.

The marked shift in reaction times observed in NHP1 during the 'induction' period of fsCT-DBS (Fig. 2*B*) was not consistently observed in NHP2 (Fig. 2*D*). However, reaction times in NHP2 were influenced by fsCT-DBS, where median reaction times between the start and trial 700 in Fig. 2D exhibit a gradual increase, from 345ms to 370ms with current levels above 1.0mA during the 'induction' phase, consistent with expected increases in reaction times in the later portions of experimental sessions; however, the variance in reaction times actually decreases, from a CV of 0.18 to 0.1. Once behavioral 'control' was established after trial 700, all reaction times are significantly slower (median 480ms, ranksum $p<0.05$) but not significantly different between subsequent ON and OFF fsCT-DBS periods (Fig. 2*D*).

During the 'induction' phase, behavioral performance was variably influenced by fsCT-DBS, except for reaction times in NHP1 (Fig. 2*B*). However as time on task increased fsCT-DBS ultimately resulted in an unexpected 'control' of behavioral performance that was tightly correlated with subsequent fsCT-DBS ON periods in both animals (Fig. 2*A*,*C*). 'Control' of behavioral performance in both animals was only achieved with fsCT-DBS and only when a rostral to caudal electric field was generated within the CT using field-shaping CT-DBS within a subset of DBS contacts. However, a directly comparable degree of behavioral control was not achieved in NHP2 and never demonstrated the robust and consistent behavioral response to fsCT-DBS, as seen regularly across the 30 months in NHP1.

Behavioral facilitation with fsCT-DBS is restricted to a range of stimulation amplitudes.

Behavioral performance in both animals was dependent on fsCT-DBS amplitude. In NHP1 (Fig. 3*A*), current levels between 1.0 and 2.5mA, following trial 450, consistently facilitate performance (green periods, positive LOR values, $p<0.05$), while current levels below or above this range have no effect on performance (gray periods, Fig. 3*A*). In NHP2, current levels from 0.25 to 1.25mA have either no effect or facilitate performance (Fig. 3*C*), while currents above 1.25mA consistently suppress performance (red colored periods, negative LOR, $p<0.05$).

The relationship between the amplitude of fsCT-DBS stimulation and performance is illustrated by the red curve in Fig. 4, a fit of a 2nd order polynomial to the distribution of LOR values (Fig. 4*A,D*). The fit demonstrates an inverted-U relationship (Yerkes and Dodson 1908; Mair et al. 2008) between stimulation amplitude and facilitation of performance in both animals. However, this relationship is restricted to amplitudes between 0.25 and 1.25mA in NHP2. In

addition, standard CT-DBS configurations also contribute to the inverted-U relationship in both animals (Fig. 4*B,E*). Overall both field-shaping and standard configurations of CT-DBS resulted in both facilitation and suppression of performance.

The average behavioral change in terms of percentage of correct trials, shown for each subset of LOR values as a function of trial number relative to DBS onset, illustrates the overall behavioral effect of CT-DBS (Fig. 4*C,F*). Each profile is normalized to pre-DBS baseline performance levels for direct comparison across CT-DBS periods. The dark green profile, corresponding to fsCT-DBS periods with significantly positive LOR values (Fig. 4*A*), demonstrates a rapid enhancement in performance that peaks at the fourth trial post DBS onset (elapsed time of ~20 seconds) and then gradually declines across the 20 trials shown (Fig. 4*C*). Of note, the decline in performance following the peak, on average, did not fall to zero during the fsCT-DBS periods used in this study. Standard CT-DBS configurations also resulted in periods of significant behavioral facilitation, however the behavioral profile shown in light blue (Fig. 4*C*) is not as robust, both in terms of the peak and the duration of the sustained performance during CT-DBS. Of note, the average behavioral profile generated by the fsCT-DBS parameter sets that produced non-significant LOR values (shown in black) exhibits an initial dip in the first trial followed by an modest increase, a profile not present in the standard CT-DBS configurations (Fig. 4*C*).

In NHP2, a similar distribution of LOR values (Fig. 4*D,E*) and corresponding average behavioral change (Fig. 4*F*) is observed, although the robust behavioral facilitation observed in NHP1 during fsCT-DBS (dark green profile in Fig. 4*C*) was not replicated in NHP2 (dark green profile in Fig. 4*F*). Both fsCT-DBS and standard CT-DBS significantly facilitated behavioral performance (light blue and dark green profiles in Fig. 4*F*), to levels comparable to standard CT-DBS in NHP1 (Fig. 4*C*). Of note, fsCT-DBS and standard CT-DBS did result in an initial dip in performance during non-significant periods (black and gray profiles in Fig. 4*F*). The critical finding here is that behavioral facilitation in NHP2 only occurred when stimulation was restricted to a subset of contacts (3, 4, and 5) on the two DBS leads indicating a narrow window of behavioral facilitation effects for this electrode configuration. We carried out computation modeling experiments (see below) to examine the relationship of this isolated effect in NHP2 and the impact of CT-DBS using the contacts producing robust behavioral facilitation in NHP1 (0, 1 and 2) during fsCT-DBS.

Behavioral facilitation is restricted to a specific polarity of fsCT-DBS

The high degree of 'control' over behavior was contingent not only on the amplitude of fsCT-DBS (Fig. 3, 4), but also on the polarity of the electric field established across the two DBS leads in both animals. In NHP1, tight coupling of behavioral performance to the ON and OFF fsCT-DBS periods (Fig. 2*B*, 3*A*, 4*C*) was observed only when the polarity of the electric field was arranged in a rostral to caudal orientation by assigning at least one of the anode(s) in the stimulation circuit to contacts 0, 1 and 2 on the rostral lead and at least one of the cathode(s) to contacts 0, 1 and 2 on the caudal lead. In NHP2 a similar relationship between the polarity of fsCT-DBS and behavioral facilitation was observed (Fig. 2*C*, Fig. 4*F*) when cathodes were placed on at least one of the upper three contacts (3, 4 and 5) of the caudal DBS leads and anodes placed on the corresponding contacts in the rostral DBS leads; the effects, however were not as robust as in NHP1. The polarity of stimulation resulted in clear differences in behavioral performance when all inter- and intra-lead CT-DBS configurations were explored in more detail in NHP1 (Fig. 8). This novel method of CT-DBS orients the electric field (Butson and McIntyre 2008; Chaturvedi et al. 2012) along the anterior-posterior axis of the brain and across a larger volume of tissue within the CT than is possible with standard CT-DBS.

Summary of the effects of field-shaping and standard CT-DBS on behavioral performance

A large set of CT-DBS parameter combinations in terms of frequency (20, 40, 150, 175, 200 and 225Hz), amplitude (0.25-3.0mA) and anode(s) and cathode(s) configurations were explored in both animals (Fig. 4). In this study, a total of 2461 DBS periods are analyzed from NHP1, each lasting an average of 32 (median of 26) trials, ranging from 20 to 500 trials in length and in NHP2 661 DBS periods are analyzed, each lasting an average of 32 (median of 31) trials, ranging from 20 to 62 trials in length. However only a subset, 123 out of 295 configurations in NHP1 and 55 out of 428 in NHP2, significantly affected behavioral performance, either resulting in facilitation (positive LOR, $p<0.05$) or suppression (negative LOR, $p<0.05$). In summary, fsCT-DBS resulted in greater facilitation of behavioral performance (947 in NHP1, 48 in NHP2) when compared to standard CT-DBS (36 in NHP1, 22 in NHP2) (Fig. 4).

LFP activity of frontostriatal recording sites during behavior

As the animals performed the vigilance task, in the absence of CT-DBS, LFP activity recorded from frontal cortices in both animals and in striatal populations in NHP1 exhibited graded and task related modulation of spectral power (Fig. 5*A,B,E,F*). A sustained increase of spectral power in the 13 – 25Hz range, 'beta-band', and a corresponding decrease of spectral

power below 10Hz during the delay period of correctly performed trials (red curve, Fig. 5*A,E*) is present when compared to the pre-delay period of InCorrect trials (blue curve, Fig. 5*A,E*). Of note, baseline and peak activity within the 'beta-band' range during both Correct and InCorrect trials is different in NHP1 compared to NHP2 (Fig. 5*A*,*E*), a phenomenon that has been reported in other NHP studies while recording from similar frontal (Dotson et al. 2014) and striatal (Courtemanche et al. 2003) locations as the animals performed similar visuomotor reaction time tasks. Enhancement of 'beta-band' LFP activity is known to occur during periods of movement planning and preparation within both frontal (Sanes and Donoghue 1993; Brovelli et al. 2004; Witham et al. 2007; Buschman and Miller 2007; Zhang et al. 2008; Verhoef et al. 2011; Buschman et al. 2012; Dotson et al. 2014) and striatal (Courtemanche et al. 2003; Bartolo et al. 2014) regions. Motor planning and preparation were two operations the NHPs had to organize to successfully complete trials in this study. On average, dynamics within LFPs recorded during the vigilance task, without CT-DBS, were consistent between the two animals (Fig. 5*B*,*F*).

Frontostriatal activity is significantly modulated by fsCT-DBS

During fsCT-DBS, 'beta-band' power generally increased and power below 10Hz generally decreased (Fig. 5*C,G*). This shift in LFP power is observed throughout the task (Fig. *5D,H*) even between trials when the animal's behavior, in the form of fixation, is not constrained. Representative frontal LFP (10-40Hz) recordings from both animals (Fig. 6A,B) illustrate the time varying dynamics of 'beta-band' activity just prior to and during fsCT-DBS. At the onset of fsCT-DBS (red line) the amplitude of the LFP immediately decreases (Fig. 6*A*), followed by a marked increase in 'beta-band' activity (Fig. 6*A,B*). To compare LFP activity during equivalent behavioral states in the two animals, analysis of LFP power spectra was restricted to the delay period of the vigilance task (Fig 1*A*). The average power spectra from two representative frontal LFP signals recorded during the delay period of correctly performed trials for each animal is shown in figure 6*C,F*. The average power spectra of the LFP during fsCT-DBS (red trace) demonstrates a significant enhancement of power within the 'beta-band', a significant decrease in lower frequency power (Fig. 6*C,F*) and a generalized increase in higher frequency power (>25Hz) in NHP1 (Fig. 6*C*) when compared to OFF periods (black trace).

In order to combine individual LFP signals across recording sites and experimental sessions, the power spectra of the LFP for each recording site were converted to a Z-score and subjected to significance testing using a two-group comparison test (t-test, $p<0.05$) (Bokil et al. 2007) and FDR ($p<0.05$) (Benjamini and Hochberg 1995) (*see Methods*). In NHP1, 3592 independent broadband signals were recorded across the 218 sessions included in this study

and here a reduced set of 2577 LFP recordings are analyzed from a subset of facilitatory fsCT-DBS configurations and amplitudes ranging from 0.75 to 3.0mA. On average, the onset of fsCT-DBS results in a robust yet transient shift in the peak of the 'beta-band' power (Fig. 6*A,D*), from ~18 to 25-30Hz within the first few trials (~5-10 seconds) which gradually settles to an enhanced level of ~18-20 Hz within the first four to five trials (~20-25 seconds) of the fsCT-DBS ON periods (Fig. 6*D*). The shift in 'beta-band' power over the subsequent ~4-5 trials following the onset of fsCT-DBS correlates well with the animal's resumption of peak behavioral performance relative to baseline (dark green curve in Fig. 4*C*). These marked changes in spectral power prior to and during fsCT-DBS are observed in both frontal and striatal recording sites in NHP1 (Fig. 7*A*,*C*).

In NHP2, fsCT-DBS induces a similar shift in the LFP power spectra recorded from the frontal cortex (Fig. 6*B*,*F*). The average Z-score of the LFP power spectra, aggregated over 60 of the 206 independent recording sites within the frontal cortex exhibits a significant enhancement of 'beta-band' power during fsCT-DBS and a significant decrease in power between 1 and 15Hz at the onset of fsCT-DBS and (Fig. 6*B*,*F*). Behavioral facilitation during fsCT-DBS in NHP2 is not as rapid (dark green curve in Fig. 3*F*) as in NHP1 and in NHP2 we also observe a weaker temporal correlation between enhanced performance and increased power within the 'beta-band' of the frontal LFPs (Fig. 6*F*).

In both animals, the degree of change in the average power spectra during fsCT-DBS correlates and grades with the amplitude of stimulation, where higher current levels result in significantly greater shifts in the distribution of the LFP power spectra (Fig 6*E*, *H*). Three sets of fsCT-DBS amplitudes levels are represented by average Z-scores and are color-coded for increased current, ranging 0.75-3.0mA (Fig 6*E*, *H*). The peaks within the 'beta-band' of the average Z-scores in NHP1 are significantly greater with a subtle shift to a higher peak frequency (Fig. 6*E*, *7B,D*) when compared to NHP2 (Fig. 6*H*), yet the trend is consistent between animals, where higher DBS amplitudes led to similar shifts in the profiles of the LFP power spectra.

Polarity of fsCT-DBS impacts performance and LFP power spectra

In addition to demonstrating robust effects of fsCT-DBS on behavioral performance and frontostriatal activity in NHP1, we discovered that the spatial arrangement and polarity of the electric field produced during fsCT-DBS play a significant role in determining the effectiveness of stimulation. Therefore, more detailed examination of fsCT-DBS and standard CT-DBS configurations were conducted within the three distal contacts (0, 1 and 2) of the two DBS leads (Fig. 8). When the electric field was applied across one of the three distal contacts of the DBS

leads in a rostral-caudal direction (‘C1’ in Fig. 8*A*) with cathode(s) assigned to the caudal lead ‘C’, (blue contacts, Fig. 8A) and anode(s) assigned to contacts 0, 1 or 2 of the rostral lead, (green contacts), an enhancement in average performance during DBS is observed (red curve ‘C1’ in Fig. 8*B*). The opposite polarity of fsCT-DBS (‘C2’ in Fig. 8*A*) resulted in a partial behavioral suppression, represented by the blue average performance curve (‘C2’ in Fig. 4*B*). When standard intra-lead CT-DBS was applied using only a single DBS lead (‘C3’ in Fig. 8*A*), performance was also suppressed, most predominantly within the first few trials as seen in the green average performance curve (‘C3’ in Fig. 8*B*). These results demonstrate that the location of the cathode and anode within a restricted region of the CT can result either in significant enhancement, no effect, or a slight suppression of performance.

Impact of bipolar anode/cathode pair on neural activity

Frontostriatal recruitment exhibited a clear dependence on the spatial arrangement of the cathode and anode pairing across the DBS leads (Fig. 8*C*). The average Z-scores of the power spectra for each subset of LFP sites recorded during the three configurations ‘C1’, ‘C2’ and ‘C3’ are shown in Fig. 8C. The configuration ‘C1’ produces a strong suppression of spectral power in the 1-15Hz range when compared to ‘C2’ and ‘C3’, and a centering of increased spectral power around 18Hz, as compared to the broader peak between 20-28Hz seen during ‘C2’ (Fig. 8*C*). The stimulation amplitude (0.75-2.5mA) and high frequency range (150-225Hz) are comparable for the three configurations, suggesting that the significant differences observed in spectral power change likely represent the impact of changing the location of the cathode in the bipolar configuration (Fig. 8*A*). Of note, with the same cathode placement, standard intra-lead CT-DBS ‘C3’ predominantly suppresses behavior and produces only a modest change in frontostriatal ‘beta-band’ LFP power when compared to fsCT-DBS ‘C1’ and ‘C2’.

Impact of multipolar anode/cathode pairs on behavior and neural activity

When two sets of cathodes and anodes (‘C4-C6’) are used, in arrangements analogous to the spatial arrangements shown in configurations ‘C1-C3’ (Fig. 8*A*) but now delivering twice the current, the animal’s behavior performance (Fig. 8*D*) and frontostriatal recruitment (Fig. 8*E*) exhibit results both similar to and different from those observed during single anode-cathode configurations. Dual rostral to caudal fsCT-DBS, configuration ‘C4’ results in robust behavioral facilitation (red profile in Fig. 8*E*) similar to ‘C1’. Interestingly, when the opposite polarity of fsCT-DBS is used, ‘C5’, the animal’s average behavioral performance, shown in blue, is also facilitated, but at a significantly lower level and with a slower rate than ‘C4’. However, the impact

of ‘C5’ is significantly different from ‘C2’ where behavior is suppressed by ‘C2’ but facilitated by ‘C5’ even though both configurations had the anode(s) located on the caudal lead (blue profiles in Fig. 8*B*,*D*). Standard intra-lead CT-DBS on both leads simultaneously, ‘C6’, results in a modest increase in the animal’s average behavioral performance, again significantly different from ‘C3’ where performance is transiently suppressed (green profiles in Fig. 8*B*,*D*).

The reversal in the behavioral performance effect between ‘C2’ and ‘C5’ and between ‘C3’ and ‘C6’, and facilitation for both ‘C1’ and ‘C4’, suggests that the link between behavioral facilitation and stimulation may reflect an interaction between a number of cellular mechanisms or cellular populations with different thresholds and sensitivities to the orientation of the electric field. Threshold for behavioral facilitation may be lowest with ‘C1’; adding additional current with ‘C4’ does not improve substantially on ‘C1’ because performance enhancement has saturated even if ‘C4’ is capable of recruiting additional neural populations (see below, and Fig. 8*C,E*). Configurations ‘C2’ and ‘C3’ suppress performance, but if enough current is available in the local environment, as with ‘C5’ and ‘C6’, there will be adequate recruitment for the enhancement of performance.

Frontostriatal recruitment during dual anode-cathode fsCT-DBS, for both configurations ‘C4’ and ‘C5’ significantly enhanced ‘beta-band’ activity and a general increase in higher frequency band power, ~30-40Hz, when compared to standard CT-DBS ‘C6’ (Fig. 8*E*). Note the near doubling in the peak of the average Z-score of the power spectra within the ‘beta-band’ during dual (‘C4’ in Fig. 8*E*) versus single (‘C1’ in Fig. 8*C*) cathode-anode fsCT-DBS (red curves in both plots), a result of doubling the current entering the CT through the addition of the second anode/cathode pair. Of note, when the current is doubled using fsCT-DBS of the opposite polarity, ‘C5’, a similar frontostriatal recruitment profile in the Z-score of the LFP power spectra to ‘C4’ is observed (Fig. 8*E*), but this profile is not a simple doubling of the activation produced by ‘C2’ which employs a single cathode-anode pair; changes in dynamics are also evident when comparing the two reverse polarity configurations ‘C2’ and ‘C5’. In general, clear differences in frontostriatal recruitment are strongly dependent on the arrangement of the cathodes and anodes within a circumscribed area of the primate CT. In NHP2, a comparable series of configurations was not conducted because the level of robust and reproducible behavioral ‘control’ achieved in NHP1 was not well established in NHP2.

Modeling of axonal fibers activated by fsCT-DBS: Evidence for a role of the DTTm.

A biophysical modeling approach (Butson et al. 2011; *see Methods*) was developed for each animal to derive the predicted locations of axonal activation during fsCT-DBS and

standard CT-DBS configurations that produced behavioral facilitation in both animals. Electric field models were combined with an NHP DTI template (Adluru et al., 2012; *see Methods*) to visualize the voltage distribution in space surrounding the DBS leads enabling a visualization of the extent of axonal activation within and around the CT targets (Fig. 9*A*).

In NHP1, two 6-contact DBS leads are positioned in the model within the right central thalamus where robust and reproducible facilitation of behavioral performance and frontostriatal recruitment were observed when the cathodes were assigned to the three distal contacts, 0, 1 and 2 of the caudal lead and the anodes were assigned to contacts 0, 1, and 2 of the rostral lead ('C1' and 'C4' in Fig. 8). An example standard bipolar configuration illustrates the field generated by a 1.5mA current applied between contacts 0 and 1 of the DBS lead, with the anode assigned to contact 1 and the cathode on contact 0, where the transparent yellow regions representing the spatial extent of the generated voltage distribution (Fig. 9*B*). The white dotted line is a schematic of a modeled axon that intersects the area of activation generated by the voltage distribution and the red segments represent stretches of the axon that are depolarized and activated by the stimulation (McIntyre et al. 2002; Butson et al. 2011). A maximum stimulation current of 1.5mA is used in the electric field models for NHP1 (Fig. 9*B,C,D,F*) since it produced consistent behavioral and physiological effects.

A broad distribution of axonal activations, identified as small yellow spheres, can be seen when all facilitatory fsCT-DBS configurations ('C1' and 'C4', Fig. 8) are combined (Fig. 9*C*). The population of axonal activation shown in Fig. 9*C* is then reduced by two additional steps of processing: 1) a DTI-derived template (Adluru et. al. 2012) of fiber orientations for the NHP (271 animals) is used to select the axon activation closest to the positions of fiber bundles in the CT; 2) all electric field models using non-facilitatory configurations and the same three distal contacts are then subtracted from the facilitatory fsCT-DBS configurations (see *Methods*). Performing a volumetric subtraction of one map from the other two combined maps allowed us to identify voxels that are activated differentially by effective fsCT-DBS (cyan points in Fig. 9*D*,*F*). As planned, contacts 0, 1 and 2 of the caudal DBS lead are located within the caudal 'wing' of the CL nucleus (Glenn and Steriade 1982) and the rostral lead is located within the lateral portion of the medial dorsal (MD) nucleus adjacent to the Pc/CL nucleus. The model-predicted axon activations within the lateral border of CL and CM/Pf and in the lateral component of the medial dorsal (MD) nucleus (a region included as part of NHP CL by some anatomists, Jones 1998) are strongly activated in NHP1 (Fig. 9*D,F*) and lie within a region that intersects a high concentration of fibers of the DTTm as it courses through the central thalamus (Edlow et al. 2012). This region is highlighted with a white oval and in the histological

reconstruction of the caudal DBS leads within the right thalami of both animals with a black-dotted oval (Fig. 10*B,C*). In summary, a total of 11 out of 12 contacts are active, 8 are located within or within range of CL and 3 contacts are out of range and unable to drive CL targets in NHP1.

In NHP2, two 6-contact DBS leads are placed into the model of the right central thalamus (Fig. 9*E,G*) and two 6-contact DBS leads are placed into the left thalamus (not shown). One DBS lead is located within left medial MD, out of range of the CT targets and therefore excluded from this study. Of the three remaining DBS leads, the upper three contacts (3, 4, and 5) of the right caudal lead and contacts 4 and 5 in the left caudal lead produced periods of behavioral facilitation and frontal recruitment during both fsCT-DBS and standard inter-lead bipolar stimulation. In NHP2, 1.0mA is used to generate the axonal activation maps for all facilitatory configurations (Fig. 9*E,G*), which are combined because a comprehensive examination of all non-effective configurations within the same set of contacts was not conducted. As planned, the caudal DBS leads in NHP2 are ~2.0mm caudal to those in NHP1, and contacts 3, 4 and 5 were caudal to the 'wing' of CL, primarily in the pulvinar, paralaminar MD and adjacent to the lateral habenula (Fig. 9*E,G*). The distal contacts of both caudal leads (0, 1 and 2) are located within the parafascicular (Pf) nucleus, and contacts 0 and 1 are located within the fasciculus retroflexus (habenula-peduncular tract) a robust bundle of fibers that traverse the center of the Pf (Sutherland 1982; Jones 2007) and stimulation results within these contacts are excluded from this study (*see Methods*).

Modeling of the activated axons in NHP2 produces a distribution of locations that differed from NHP1, consistent with the reduced efficacy of facilitatory fsCT-DBS in NHP2 (Fig. 9*E,G*). In NHP2, fsCT-DBS within the upper three contacts 3, 4 and 5, resulted in behavioral facilitation (Fig. 2*D*, 4*F*) and graded activation within the frontal cortex, assessed through LFP recordings (Fig. 5*E*,*F*, 6*F,G, H*). Overall fsCT-DBS between the two DBS leads in NHP2 produces axonal activation maps that marginally overlapped with those generated in NHP1 (Fig. 9*D,F*) and as a consequence a significantly smaller number of putative DTTm fibers are activated and these configurations produce minimal activation of axons in paralaminar MD. Thus, the ~2.0mm posterior and 1.0mm medial difference in the activation of CT targets in NHP2 relative to NHP1 likely limited the recruitment and/or 'activation' of DTTm fibers. In NHP2, a total of 15 out of 18 contacts were active, 8 were located within or within range of activating CL targets. In summary, 16 independent CT locations within 3 central thalami across 2 animals were included in this study and the locations of the DBS leads relative to the targeted CT nuclei

and en passant fiber tracts of the DTTm used to center the biophysical models were confirmed through standard myelin and Nissl staining (Fig. 10*B*, *C*, *see Methods*).

Discussion

In this study we sought to determine if electric stimulation of nuclear targets within the central thalamus of healthy NHPs could modulate endogenous arousal and behavioral performance during goal-directed behaviors. We find strong evidence in two healthy NHPs that a specific region of the central thalamus, the 'wing' of CL and paralaminar MD (Jones 2007) and the DTTm (Edlow et al. 2012), can be electrically stimulated to facilitate performance on vigilance tasks (Fig. 2-4) and a novel method of DBS, field-shaping CT-DBS, that isolates anodes and cathodes on spatially separate DBS leads, when applied to this area of the CT, more robustly and reliably enhances behavioral performance and modulates endogenous arousal (Fig. 5-8).

Our biophysical modeling (Fig. 9) and histological (Fig. 10) studies concordantly identify this select region within the central thalamus that includes fibers of the DTTm (Edlow et al. 2012) and cell bodies of the large lateral 'wing' of the central lateral nucleus and paralaminar MD (Jones 2007) as the likely source of the facilitatory effect of fsCT-DBS. The DTTm is a diverse aggregate of excitatory efferent projections, including CT thalamocortical and thalamostriatal efferents and en passant fibers projecting from brainstem arousal systems (Edlow et al. 2012) that broadly innervate regions of cortex and striatum (Jones 2007). By broadly sampling large-scale neuronal populations in the frontal cortex and striatum, we show that behavioral modulation coincides with consistent shifts in LFP power spectra in both NHPs during fsCT-DBS (Fig. 5, 6). The shift in LFP power spectra is linked to improved performance during fsCT-DBS, in both animals, and is characterized by a marked decrease of low-frequency power below 15Hz and an elevation of 'beta-band' (~15-25Hz) (Fig. 5, 6) and higher frequency power (~30-40Hz) in NHP1 (Fig. 5, 6, 7, 8). Redistribution of LFP power is also observed during task performance without DBS in both animals when attentional resources are maximally allocated during the delay period of a correct trial, as compared to LFP power during inter-trial intervals when attention is less focused (Fig. 5*A,B*,*E,F*; cf. Schiff et al. 2013). The comparable shift in overall spectral power from lower (<15Hz) to higher (>15Hz) frequencies supports our inference that fsCT-DBS produces effects similar to endogenous arousal regulation, although power increases are nominally greater between ON and OFF fsCT-DBS periods than between attentive and inattentive states during unstimulated trials (Fig 5*A,E*). As a consequence, we hypothesize that facilitatory fsCT-DBS produces a significant increase in the afferent drive to the

anterior forebrain (Fig. 10*A*) supporting cognitive processes that maintain performance over extended periods of time.

fsCT-DBS recapitulates endogenous arousal regulation.

Arousal regulation optimizes sustained attention and readiness for action by both facilitating patterns of brain activity that promote alertness while damping those linked to drowsiness (Schiff 2008). Our LFP results support the rapid action of fsCT-DBS on arousal regulation. During the delay period of the vigilance task, in the absence of fsCT-DBS, the ratio of spectral LFP power in lower frequencies (<15 Hz) to higher frequencies (>15 Hz) changes during a correctly performed trial (Fig. 5*B*, *F*) and this shift is further enhanced with fsCT-DBS (Fig. 5*C*, *G*). Historically, the LFP has been thought to reflect integrated synaptic and dendritic activity (Mitzdorf 1985); here we interpret our results through a more modern interpretation of LFP activity as an indirect measure of local excitatory-inhibitory circuit processing (Buzsaki et al. 2012) that is tightly correlated with gradations in firing rates of local neuronal populations (Goense and Logothetis 2008). Therefore, we infer that fsCT-DBS promotes a rapid state change (Harris and Thiele 2011) across the anterior forebrain through direct activation of CT efferent axons that broadly synapse within the frontal and striatal areas sampled in this study (Jones 2007) (Fig. 10*A*). The simultaneous decrease of low frequency power (<15Hz) and enhancement of higher frequency power within the 'beta-band' (>15Hz) of the LFP during task execution constitutes a shift in network dynamics that recapitulates changes that accompany native increases in arousal and performance (Steriade 1996; Jung et al. 1997). The dynamics of this shift in network activity is consistent with the well-established phenomenon of cortical activation through electric stimulation of the central thalamus (Moruzzi and Magoun 1949) and/or ascending reticular arousal system (Moruzzi and Magoun 1949; Munk et al. 1996). Therefore, we hypothesize that fsCT-DBS likely shifts recipient cellular populations of the anterior forebrain into a high conductance state (Steriade et al. 1996; Destexhe et al. 2003; Rudolph et al. 2005), reflected in the rapid and persistent change of the power spectra recorded in the frontostriatal LFPs (Fig. 5-8). Of note, the rapid activation of frontal and striatal areas during graded levels of site specific fsCT-DBS is reminiscent of short latency diffuse cortical responses elicited by graded electrical stimulation within distinct regions of the diffuse thalamic system in anesthetized cats (Hanbery and Jasper 1953).

The discovery that a series of fsCT-DBS periods led to a 'control' phase lacks a mechanistic understanding and without suitable measurement of activity within the larger arousal regulation network, comprising the central thalamus and anterior forebrain areas, it will

remain until further studied. However when the animals were in the 'control' phase and ceased to perform during OFF fsCT-DBS periods, they did work for water rewards when either enough time had elapsed between fsCT-DBS periods (Fig. 2*A*, *C*) or when a large bolus of water (1-2cc) was freely delivered by the investigators, which 'coaxed' the animals into re-engaging with the task. These observations, albeit not well controlled and/or quantified, are intriguing and somewhat comparable to studies conducted in cats performing bar presses for milk rewards during cryogenic blockade of the inferior thalamic peduncle (ITP), a fiber bundle containing arousal regulating intralaminar fibers projecting to the orbitofrontal cortices (*see Figure 13* in Skinner and Yingling 1977).

The sensitivity of behavior and frontostriatal activation to the polarity of fsCT-DBS.

The strong anisotropic specificity of fsCT-DBS demonstrated in NHP1 (Fig. 8) has broader implications for the technique of deep brain stimulation. Butson and McIntyre (2008) developed theoretical results supporting the potential value of 3-D current steering in DBS; modeling current flow through adjacent cathodes showed that increasing the magnitude of the volume of tissue activation could be achieved when compared to monopolar stimulation methods. Theoretically these results suggest that field-shaping may constitute a more robust and reliable DBS method in applications where a diffuse fiber bundle and/or pathway is targeted within a heterogeneous tissue space, such as the subcallosal cingulate, a promising DBS target for treatment resistant depression (Riva-Posse et al. 2014). Here, direct comparisons of behavioral outcomes and frontostriatal LFP activity using standard CT-DBS and field-shaping CT-DBS configurations applied in the same fixed in-situ DBS system demonstrate these anticipated advantages for developing next-generation DBS systems to stimulate new targets in emerging treatment resistant indications.

Frequency dependent effects of fsCT-DBS.

Our behavioral and physiological findings during high frequency fsCT-DBS are consistent with evidence from recent optogenetic fMRI experiments that demonstrate significant and reliable frequency dependence of recruitment of frontostriatal populations with direct optogenetic activation of principal neurons in the central lateral nucleus (Liu et al., 2015), the primary CT nuclear target in this study. Overall, the high frequency dependent effects shown here (150-225Hz) are also consistent with experimental and clinical CT-DBS studies where greater effectiveness with high frequency stimulation (>100 Hz) has been demonstrated (Shirvalkar et al. 2006; Schiff et al. 2007; Mair and Hembrook 2011). The central median (CM) -

982 parafascicular (Pf) nuclear complex (CM-Pf), the caudal component of CT, is a promising DBS
983 target for the treatment of Tourette's syndrome, and in a recent large animal fMRI study (Kim et
984 al. 2013), DBS of CM and Pf demonstrated a clear frequency dependent activation (130Hz
985 versus 60Hz) of target structures within the cortex and striatum. In primates CM-Pf provides the
986 bulk of synaptic input to basal ganglia (Parent and Parent 2005; Jones 2007) and recent
987 optogenetic studies demonstrate clear physiological differences in CL versus Pf inputs onto
988 medium spiny neurons of the rodent striatum (Ellender et al., 2013).

989 As with many instrumented behavioral tasks, analysis of the reaction times of the NHPs
990 in this study opens CT-DBS to mechanistic interpretation. In NHP1, low frequency (20 and
991 40Hz) fsCT-DBS stimulation had a strong effect of reducing reaction times in aggregate
992 (ranksum, $p<0.05$), where median reaction time was 360ms (20-40Hz) compared to 385ms
993 (150-225Hz) and 410ms during OFF fsCT-DBS periods; however this result was not observed in
994 NHP2 (median of 365±5ms). This effect may relate to antidromic activation of neurons within the
995 pedunculopontine nucleus that peak in response to electric stimulation around ~40-50Hz
996 (Kezunovic et al. 2011). Entrainment of these neurons through DBS could facilitate early
997 reaction times via outflow from the brainstem or basal ganglia structures (Garcia-Rill et al.
998 2014). Alternatively, central lateral neurons of the CT predominantly fire at rates between 20
999 and 40Hz during wake states (Glenn and Steriade 1982; Steriade et al. 1993), thus 20 and
1000 40Hz fsCT-DBS during behavioral performance may entrain and thereby enhance these intrinsic
1001 intrathalamic firing dynamics (Steriade et al., 1996, Steriade 2000).

1002 High frequency (>100Hz) DBS within subcortical targets robustly alleviates Parkinsonian
1003 symptoms in patients (Vitek et al. 2008; Montgomery and Gale 2008) and MPTP treated NHPs
1004 (Johnson et al. 2009) whereas low frequency DBS (10-30Hz) can exacerbate symptoms (Florin
1005 et al. 2008; Johnson et al. 2009; Chen et al. 2011; McCracken and Kiss 2014) through
1006 entrainment that enhances pathological 'beta-band' oscillatory activity (Brown 2009; Jenkinson
1007 and Brown 2011). As of yet, it is unclear exactly how stimulation with low frequencies (20 and
1008 40Hz) produces faster reaction times as compared with stimulation with high frequencies (150-
1009 225Hz) in NHP1.

1010 Performance enhancement and recruitment of frontal circuits during the vigilance task
1011 with fsCT-DBS may be linked to the high-thresholds for dendritic electrogenesis in L2/3 and L5
1012 cortical pyramidal cells (Larkum et al. 1999, 2007, 2009). Dendritic potentials and calcium
1013 transients are generated in L2/3 pyramidal neurons when the frequency of depolarizing inputs
1014 exceeds a critical value of 130 Hz (Larkum et al. 2007). Therefore, high frequency fsCT-DBS
1015 may initiate cortical activation in supra- and infragranular layers through the direct stimulation of

thalamocortical CT axons that predominantly innervate the upper layers of cortex (Llinás et al. 2002, Jones 2007), where the bulk of L2/3 and L5 dendritic arbors are located, thereby promoting corticocortical communication (Purpura and Schiff, 1997). While our microelectrode recording methods cannot resolve the pattern of laminar specificity, recent studies in the mouse using optogenetic stimulation of CT efferents demonstrate a preferred activation of supragranular cortical regions and diffuse anatomical innervations of Layer I by transduced CT neurons (Cruikshank et al. 2012). Therefore greater activation of fibers within the DTTm (Fig. 9, 10*A*) and CT targets with increasing levels of current (Fig. 6, 7, 8) may likely account for the robust and rapid shifts in behavioral performance and changes in LFP power spectra observed during fsCT-DBS.

Limitations and future directions

The primary goal of this study was to explore, for the first time, the effects of CT-DBS in intact and behaving NHPs. A statistically rigorous characterization of behavioral and physiological effects during all possible CT-DBS configurations was not feasible given the fixed number of DBS leads, active contacts and locations attempted (16 independent locations) within three central thalami of two NHPs. Stimulation of adjacent thalamic nuclei and off-target effects that interfered with behavioral performance were pronounced in NHP2, precluding a comprehensive exploration of all possible CT-DBS configurations that produced facilitation in this animal, when compared to NHP1. Additional animals implanted bilaterally with multiple DBS leads in various field-shaping geometries relative to the central thalamic targets would allow for a more comprehensive investigation of this heterogeneous target, a target that spans approximately 5x8x9mm in the NHP thalamus.

The biophysical model used in this study incorporated an average (271 NHPs) DTI template (Adluru, 2012) to estimate the animal specific axon activation maps (Fig. 9). The template was used as a best estimate and registered to each animal using previously published algorithms (Viola and Wells, 1997) used in human DBS studies (Butson et al, 2007, 2011). In future studies, animal specific DTI could be combined with a high-resolution NHP DTI atlas (Calabrese et al., 2015) to optimize DBS lead implantation, post-implant visualization, and to explore the stimulation parameter space, as is being done with human subjects (Butson et al., 2011). Lastly, in order to provide a better mechanistic understanding of the polarity of the field-shaping results, measurement of brain wide activity (fMRI, PET) and central thalamic fiber tract tracing would be necessary to attempt to explain this phenomenon.

In this study we infer that the measured shifts in the power spectra of frontal and striatal LFPs during CT-DBS reflect changes in local cellular spiking activity (*see Methods*). DBS pulse shapes (biphasic 100us pulses) used in other NHP studies combined with blanking algorithms (Hashimoto et al., 2002; McCairn and Turner 2009) could be used in future studies to directly assess changes in spike timing and firing rate during CT-DBS. However, noninvasive measures could be used to assess changes in global brain activity.

Recent studies in awake and behaving rodents (reviewed in McGinley et al., 2015) and NHPs (Bouret and Richmond 2015; Varazzani et al., 2015; Joshi et al., 2016) have linked cortical 'substates' within wakefulness to marked changes in pupil diameter, muscle tone, movement, task effort and engagement to cellular membrane potentials, LFP spectral power and cortical and subcortical firing rates. The dynamics of the locus coeruleus-norepinephrine (LC-NE) system contribute to arousal, attention and motivation, and activity within the LC-NE system is associated with shifts in arousal, task performance, level of effort and motivation. Of particular relevance to the work here, firing rates of LC neurons are tightly linked to changes in pupil diameter and behavioral performance in NHPs (Aston-Jones and Cohen 2005; Bouret and Richmond 2015; Varazzani et al., 2015; Joshi et al., 2016). In the context of our study, the LC fibers are a component of the DTTm (Edlow et al., 2012) and LC neurons send dense projections to the intralaminar and reticular nuclei of the thalamus (Pare et al., 1988; Steriade et al. 1988) and were likely activated during CT-DBS. Pupillometry, as a noninvasive and objective measure of cortical 'substates' during wakefulness (McGinley et al., 2015), could be used during DBS lead implantation to provide an addition assessment of arousal regulation during CT-DBS in NHPs and in future SBI patients undergoing CT-DBS therapy.

Implications for the development of CT-DBS as a therapeutic intervention following severe brain injury.

Collectively, our findings in healthy behaving adult NHPs demonstrate that CT-DBS, in principle, may generalize as a therapy for select SBI patients suffering from the persistent cognitive deficits resulting from SBI (Schiff and Purpura 2002; Schiff 2012). Life-long cognitive impairments following SBI are linked to general capacities for sustained attention, working memory, arousal regulation and information-processing speed (Van der Werf et al. 2000, 2003; Dikmen et al 2003; 2009; Ziino and Ponsford 2006; Ponsford 2013; Corrigan et al. 2014). Sustained attention is a foundational executive function underlying a wide-range of goal-directed behaviors that draw upon frontal-striatal-thalamic networks to maintain performance (Sarter et al. 2006). Therefore, the development of CT-DBS as a therapy for a range of cognitive

dysfunctions following SBI is supported by the hypothesis that by increasing background synaptic drive to the anterior forebrain in the partially deafferented brain of select SBI patients, it may be possible to restore frontostriatal resources underlying many cerebral integrative functions and significantly improve quality of life for a large cohort of SBI patients.

Acknowledgments:

We thank the veterinary staff of the Research Animal Resource Center at Weill Cornell Medical College for their exceptional care of the animals used in this study. We thank members of Bijan Pesaran's lab at NYU for insightful comments on preliminary results.

Grants

The National Institute of Neurological Disorders and Stroke supported this work under grant number RO1 NS067249. SCIRun was provided by a grant from the National Institute of General Medical Sciences of the National Institutes of Health under grant number P41 GM103545-17.

Disclosures

Dr. Butson has served as a consultant for IntElect Medical, NeuroPace, Advanced Bionics, St. Jude Medical, Boston Scientific and Functional Neuromodulation and is an inventor of several patents related to neuromodulation therapy. Dr. Schiff has served as a consultant for IntElect Medical and is an inventor of several patents related to neuromodulation therapy. Dr. Purpura is an inventor of several patents related to neuromodulation therapy. All other authors declare no competing financial interests.

References

Adams JH, Graham DI, Jennett B. The neuropathology of the VS after acute insult. *Brain* 123, 1327–1338. (2000)

Adluru N, Zhang H, Fox AS, Shelton SE, Ennis CM, Bartosic AM, Oler JA, Tromp DPM, Zakszewski E, Gee JC, Kalin NH, Alexander AL. A diffusion tensor brain template for rhesus macaques. *NeuroImage* 59, 306–318. (2012)

Andersen RA, Cui H. Intention, action planning, and decision making in parietal-frontal circuits. *Neuron*, *63*(5), 568-583. (2009)

Aston-Jones G Cohen JD. An integrative theory of locus coeruleus-norepinephrine function: adaptive gain and optimal performance. *Annu. Rev. Neurosci.*, *28*, pp.403-450. (2005)

Bartolo R, Prado L, Merchant H. Information processing in the primate basal ganglia during sensory-guided and internally driven rhythmic tapping. J Neurosci 34:3910 –3923. (2014)

Benjamini Y, Hochberg Y. Controlling the false discovery rate: a practical and powerful approach to multiple testing. *Journal of the Royal Statistical Society* 289-300. (1995)

Bokil H, Purpura KP, Schoffelen JM, Thomson D, Mitra P. Comparing spectra and coherences for groups of unequal size. *Journal of Neuroscience Methods* 159, 337–345. (2007)

Bouret S, Richmond BJ. Sensitivity of locus ceruleus neurons to reward value for goal-directed actions. *The Journal of Neuroscience*, *35*(9), pp.4005-4014. (2015)

Brovelli A, Ding M, Ledberg A, Chen Y, Nakamura R, Bressler SL. Beta oscillations in a large-scale sensorimotor cortical network: directional influences revealed by Granger causality. *Proceedings of the National Academy of Sciences* 101(26), 9849-9854. (2004)

Brown P. Abnormal oscillatory synchronisation in the motor system leads to impaired movement. *Curr. Opin. Neurobiol.* 17, 656–664. (2007).

Buschman TJ, Miller EK. Top-down versus bottom-up control of attention in the prefrontal and posterior parietal cortices. *Science* 315(5820), 1860-1862. (2007)

Buschman TJ, Denovellis EL, Diogo C, Bullock D, Miller EK. Synchronous oscillatory neural ensembles for rules in the prefrontal cortex. *Neuron*, *76*(4), 838-846. (2012)

Butson CR, McIntyre CC. Tissue and electrode capacitance reduce neural activation volumes during deep brain stimulation. Clin Neurophysiol. 116:2490–2500. (2005)

Butson CR, Cooper SE, Henderson JM, McIntyre CC. Patient-specific analysis of the volume of tissue activated during deep brain stimulation. *NeuroImage*, 34(2), 661–70. (2007)

Butson CR, McIntyre CC. Differences among implanted pulse generator waveforms cause variations in the neural response to deep brain stimulation. *Clinical Neurophysiology* 118(8), 1889-1894. (2007)

Butson CR, McIntyre CC. Current steering to control the volume of tissue activated during deep brain stimulation. *Brain Stimulation* 1, 7–14. (2008)

Butson CR, Cooper SE, Henderson JM, Wolgamuth B, McIntyre CC. Probabilistic Analysis of Activation Volumes Generated During Deep Brain Stimulation. *NeuroImage* 54, 2096–2104. (2011)

Buzsáki G, Anastassiou CA, Koch C. The origin of extracellular fields and currents—EEG, ECoG, LFP and spikes. *Nature Reviews Neuroscience* 13(6), 407-420. (2012)

Calabrese E, Badea A, Coe CL, Lubach GR, Shi Y, Styner MA Johnson GA. A diffusion tensor MRI atlas of the postmortem rhesus macaque brain. *Neuroimage*, *117*, pp.408-416. (2015)

Castaigne P, Lhermitte F, Buge A, Escourolle R, Hauw JJ, Lyon-Caen O. Paramedian thalamic and midbrain infarcts: clinical and neuropathological study. *Annals of Neurology* 10(2), 127-148. (1981)

Chaturvedi A, Foutz JT, McIntyre CC. Current steering to activate targeted neural pathways during deep brain stimulation of the subthalamic region. *Brain stimulation* 5(3), 369-377. (2012)

Chen CC, Lin WY, Chan HL, Hsu YT, Tu PH, Lee ST, Chiou SM, Tsai CH, Lu CS, Brown P. Stimulation of the subthalamic region at 20Hz slows the development of grip force in Parkinson's disease. *Experimental neurology*, *231*(1), 91-96. (2011)

Corrigan JD, Cuthbert JP, Harrison-Felix C, Whiteneck GG, Bell JM, Miller AC, Pretz CR. US population estimates of health and social outcomes 5 years after rehabilitation for traumatic brain injury. *The Journal of Head Trauma Rehabilitation* 29(6), E1-E9. (2014)

Courtemanche R, Fujii N, Graybiel AM. Synchronous, focally modulated β-band oscillations characterize local field potential activity in the striatum of awake behaving monkeys. *The Journal of Neuroscience* 23(37), 11741-11752. (2003)

Cruikshank SJ, Ahmed OJ, Stevens TR, Patrick SL, Gonzalez AN, Elmaleh M, Connors BW. Thalamic control of layer 1 circuits in prefrontal cortex. *The Journal of Neuroscience*, 32(49), 17813-17823. (2012)

Davies DR, Parasuraman R. *The Psychology of Vigilance.* Academic Press, London. (1982)

Destexhe A, Rudolph M, Pare D. The high-conductance state of neocortical neurons in vivo. *Nature Reviews Neuroscience* 4, 739–751. (2003)

Dikmen SS, Machamer JE, Powell JM, Temkin NR. Outcome 3 to 5 years after moderate to severe traumatic brain injury. *Archives of Physical Medicine and Rehabilitation* 84, 1449-1457. (2003)

Dikmen SS, Corrigan JD, Levin HS, Machamer J, Stiers W, Weisskopf MG. Cognitive outcome following traumatic brain injury. The Journal of head trauma rehabilitation. Nov 1;24(6):430-8. (2009)

Dotson NM, Salazar RF, Gray CM. Frontoparietal Correlation Dynamics Reveal Interplay between Integration and Segregation during Visual Working Memory. *The Journal of Neuroscience* 34(41), 13600-13613. (2014)

Elder CM, Hashimoto T, Zhang J, Vitek JL. Chronic implantation of deep brain stimulation leads in animal models of neurological disorders. *Journal of Neuroscience Methods* 142: 11–16. (2005)

Edlow BL, Takahashi E, Wu O, Benner T, Dai G, Bu L, Grant PE, Greer DM, Greenberg SM, Kinney HC, Folkerth RD. Neuroanatomic connectivity of the human ascending arousal system critical to consciousness and its disorders. *Journal of Neuropathology and Experimental Neurology* 71(6), 531-546. (2012)

Ellender TJ, Harwood J, Kosillo P, Capogna M, Bolam JP. Heterogeneous properties of central lateral and parafascicular thalamic synapses in the striatum. *The Journal of physiology*, *591*(1), pp.257-272. (2013)

Erez Y, Tischler H, Moran A, Bar-Gad I. Generalized framework for stimulus artifact removal. *Journal of Neuroscience Methods* 191(1), 45-59. (2010)

Florin E, Reck C, Burghaus L, Lehrke R, Gross J, Sturm V, Timmermann L. Ten Hertz thalamus stimulation increases tremor activity in the subthalamic nucleus in a patient with Parkinson's disease. *Clinical neurophysiology*, *119*(9), 2098-2103. (2008)

Fridman EA, Schiff ND. Neuromodulation of the conscious state following severe brain injuries. *Current Opinion in Neurobiology* 29, 172-177. (2014)

Garcia L, Audin J, D'Alessandro G, Bioulac B, Hammond C. Dual effect of high-frequency stimulation on subthalamic neuron activity. *The Journal of Neuroscience* 23(25), 8743-8751. (2003)

Garcia L, D'Alessandro G, Fernagut PO, Bioulac B, Hammond C. Impact of high-frequency stimulation parameters on the pattern of discharge of subthalamic neurons. *Journal of Neurophysiology* 94(6), 3662-3669. (2005)

Garcia-Rill E, Hyde J, Kezunovic N, Urbano FJ, Petersen E. The physiology of the pedunculopontine nucleus: implications for deep brain stimulation. *Journal of Neural Transmission* 1-11. (2014)

Glenn LL, Steriade M. Discharge rate and excitability of cortically projecting intralaminar thalamic neurons during waking and sleep states. *The Journal of Neuroscience*, *2*(10), 1387-1404. (1982)

Goense J, Logothetis NK. Neurophysiology of the BOLD fMRI signal in awake monkeys. *Current Biology* 18(9), 631-640. (2008)

Gummadavelli A, Motelow JE, Smith N, Zhan Q, Schiff ND, Blumenfeld H. Thalamic stimulation to improve level of consciousness after seizures: Evaluation of electrophysiology and behavior. *Epilepsia*, *56*(1), 114-124. (2015)

Hanbery J, Jasper H. Independence of diffuse thalamocortical projection system shown by specific nuclear destructions. *Journal of neurophysiology*, *16*(3), pp.252-271. (1953)

Harris KD, Thiele A. Cortical state and attention. *Nature Reviews Neuroscience* 12, 509-523. (2011)

Hashimoto T, Elder CM, Vitek JL. A template subtraction method for stimulus artifact removal in high-frequency deep brain stimulation. *Journal of Neuroscience Methods* 113(2), 181-186. (2002)

Hashimoto T, Elder CM, Okun MS, Patrick SK, Vitek JL. Stimulation of the subthalamic nucleus changes the firing pattern of pallidal neurons. *The Journal of Neuroscience* 23(5), 1916-1923. (2003)

Hikosaka O, Wurtz RH. Visual and oculomotor functions of monkey substantia nigra pars reticulata. III. Memory-contingent visual and saccade responses. *Journal of Neurophysiology* 49:1268–1284. (1983)

Hines M, Carnevale N. The NEURON simulation environment. *Neural Computation* 9, 1179–1209. (1997)

Jenkinson N, Brown P. New insights into the relationship between dopamine, beta oscillations and motor function. *Trends in neurosciences*, *34*(12), 611-618. (2011)

Johnson MD, Vitek JL, McIntyre CC. Pallidal stimulation that improves parkinsonian motor symptoms also modulates neuronal firing patterns in primary motor cortex in the MPTP-treated monkey. *Experimental neurology*, *219*(1), 359-362. (2009)

Jones EG. *The Thalamus, 2nd edition*. Cambridge University Press, Cambridge. (2007)

Joshi S, Li Y, Kalwani RM, Gold JI. Relationships between pupil diameter and neuronal activity in the locus coeruleus, colliculi, and cingulate cortex. *Neuron*, *89*(1), pp.221-234. (2016)

Jung TP, Makeig S, Stensmo M, Sejnowski TJ. Estimating alertness from the EEG power spectrum. *IEEE Transactions on Biomedical Engineering* 44(1), 60-69. (1997)

Kezunovic N, Urbano FJ, Simon C, Hyde J, Smith K, Garcia-Rill E. Mechanism behind gamma band activity in the pedunculopontine nucleus. *European Journal of Neuroscience*, *34*(3), 404-415. (2011)

Kim JP, Min HK, Knight EJ, Duffy PS, Abulseoud OA, Marsh MP, Kelsey K, Blaha CD, Bennet KE, Frye MA, Lee KH. Centromedian-parafascicular deep brain stimulation induces differential functional inhibition of the motor, associative, and limbic circuits in large animals. *Biological psychiatry*, *74*(12), 917-926. (2013)

Kinomura S, Larsson J, Gulyás B, Roland PE. Activation by attention of the human reticular formation and thalamic intralaminar nuclei. *Science* 271(5248), 512-515. (1996)

Larkum ME, Zhu JJ, Sakmann B. A new cellular mechanism for coupling inputs arriving at different cortical layers. *Nature* 398(6725), 338-341. (1999)

Larkum ME, Waters J, Sakmann B, Helmchen F. Dendritic spikes in apical dendrites of neocortical layer 2/3 pyramidal neurons. *The Journal of Neuroscience* 27(34), 8999-9008. (2007)

Larkum ME, Nevian T, Sandler M, Polsky A, Schiller J. Synaptic integration in tuft dendrites of layer 5 pyramidal neurons: a new unifying principle. *Science* 325(5941), 756-760. (2009)

Lempka SF, Johnson MD, Miocinovic S, Vitek JL, McIntyre CC. Current-controlled deep brain stimulation reduces in vivo voltage fluctuations observed during voltage-controlled stimulation. *Clinical Neurophysiology* 121(12), 2128-2133. (2010)

Levine B, Black SE, Cheung G, Campbell A, O'Toole C, Schwartz ML. Gambling task performance in traumatic brain injury: relationships to injury severity, atrophy, lesion location, and cognitive and psychosocial outcome. *Cognitive and Behavioral Neurology* 18, 45-54. (2005)

Little DM, Kraus MF, Joseph J, Geary EK, Susmaras T, Zhou XJ, Pliskin N, Gorelick PB. Thalamic integrity underlies executive dysfunction in traumatic brain injury. Neurology 74:558–564. (2010)

Liu J, Lee HJ, Weitz AJ, Fang Z, Lin P, Choy MK, Fisher R, Pinskiy V, Tolpygo A, Mitra P, Schiff ND, Lee JH. Frequency-selective control of cortical and subcortical networks by central thalamus. *eLife* 4:e09215. (2015)

Llinás RR, Leznik E, Urbano FJ. Temporal binding via cortical coincidence detection of specific and nonspecific thalamocortical inputs: a voltage-dependent dye-imaging study in mouse brain slices. *Proceedings of the National Academy of Sciences* 99(1), 449-454. (2002)

Luce RD. *Response times: Their role in inferring elementary mental organization*. Oxford University Press. New York, New York. (1984)

Macchi G, Bentivoglio M. The thalamic intralaminar nuclei and the cerebral cortex. In *Sensory-Motor Areas and Aspects of Cortical Connectivity* (pp. 355-401). Springer US. (1986)

Mair RG, Hembrook JR. Memory enhancement with event-related stimulation of the rostral intralaminar thalamic nuclei. Journal of Neuroscience 28, 14293-14300. (2008)

Mair RG, Onos KD, Hembrook JR. Cognitive activation by central thalamic stimulation: the Yerkes-Dodson law revisited. *Dose-Response* 9(3), 313-331. (2011)

Matsumoto N, Minamimoto T, Graybiel AM, Kimura M. Neurons in the thalamic CM-Pf complex supply striatal neurons with information about behaviorally significant sensory events. *Journal of Neurophysiology* 85, 960–976. (2001)

Maxwell WL, MacKinnon MA, Smith DH, McIntosh TK, Graham DI. Thalamic nuclei after human blunt head injury. *Journal of Neuropathology & Experimental Neurology* 65(5), 478-488. (2006)

McCairn K, Turner R. Deep brain stimulation of the globus pallidus internus in the parkinsonian primate: local entrainment and suppression of low-frequency oscillations. J. Neurophysiol. 101, 1941–1960. (2009)

McCracken CB, Kiss ZHT. Time and Frequency-Dependent Modulation of Local Field Potential Synchronization by Deep Brain Stimulation. PLoS ONE 9(7): e102576. doi:10.1371/journal.pone.0102576. (2014)

McGinley MJ, Vinck M, Reimer J, Batista-Brito R, Zagha E, Cadwell CR, Tolias AS, Cardin JA McCormick DA. Waking state: rapid variations modulate neural and behavioral responses. *Neuron*, *87*(6), pp.1143-1161. (2015)

McIntyre CC, Richardson AG, Grill WM. Modeling the Excitability of Mammalian Nerve Fibers: Influence of Afterpotentials on the Recovery Cycle. *Journal of Neurophysiology* 87, 995–1006. (2002)

McIntyre CC, Savasta M, Kerkerian-Le Goff L, Vitek JL. Uncovering the mechanism(s) of action of deep brain stimulation: activation, inhibition, or both. *Clinical Neurophysiology* 115(6), 1239-1248. (2004)

Merrill DR, Bikson M, Jefferys JG. Electrical stimulation of excitable tissue: design of efficacious and safe protocols. *Journal of neuroscience methods* 141(2), 171-198. (2005)

Minamimoto T, Kimura M. Participation of the thalamic CM-Pf complex in attentional orienting. *Journal of Neurophysiology* 87, 3090–3101. (2002)

Minamimoto T, La Camera G, Richmond BJ. Measuring and modeling the interaction among reward size, delay to reward, and satiation level on motivation in monkeys. *Journal of neurophysiology* 101(1), 437-447. (2009)

Miocinovic S, Lempka SF, Russo GS, Maks CB, Butson CR, Sakaie KE, Vitek JL, McIntyre CC. Experimental and theoretical characterization of the voltage distribution generated by deep brain stimulation. *Exp Neurol*, *216*(1), 166–76. (2009)

Mitra PP, Pesaran B. Analysis of dynamic brain imaging data. *Biophysical Journal* 76,691–708. (1999)

Mitra PP, Bokil H. *Observed Brain Dynamics*. Oxford University Press, Oxford. (2008)

Montgomery EB, Gale JT. Mechanisms of action of deep brain stimulation (DBS). *Neuroscience & Biobehavioral Reviews 32*(3), 388-407. (2008)

Moruzzi G, Magoun HW. Brain-stem reticular formation and activation of the EEG. *Electroencephalography of Clinical Neurophysiology* 1, 455-473. (1949)

Mitzdorf U, Current source density method and application in cat cerebral cortex: investigation of evoked potentials and EEG phenomena. *Physiological reviews*, *65*(1), 37-100. (1985)

Munk MH, Roelfsema PR, Konig P, Engel AK, Singer W. Role of reticular activation in the modulation of intracortical synchronization. *Science* 272, 271–274. (1996)

Nowak LG, Bullier J. Axons, but not cell bodies, are activated by electrical stimulation in cortical gray matter. II. Evidence from selective inactivation of cell bodies and axon initial segments. *Experimental Brain Research* 118(4) 489–500. (1998)

Pare D, Smith Y, Parent A, Steriade M. Projections of brainstem core cholinergic and non-cholinergic neurons of cat to intralaminar and reticular thalamic nuclei. *Neuroscience*, *25*(1), pp.69-86. (1988)

Parent M and Parent A. Single-axon tracing and three-dimensional reconstruction of centre médian-parafascicular thalamic neurons in primates. *Journal of Comparative Neurology*, *481*(1), pp.127-144. (2005)

Paus T, Zatorre R, Hofle N, Caramanos Z, Gotman J, Petrides M, Evans A. Time-related changes in neural systems underlying attention and arousal during the performance of an auditory vigilance task. *Journal of Cognitive Neuroscience* 9(3), 392-408. (1997)

Paxinos G, Huang XF, Toga AW. The rhesus monkey brain in stereotaxic coordinates. (1999)

Pesaran B, Nelson MJ, Andersen RA. Free choice activates a decision circuit between frontal and parietal cortex. *Nature*, *453* (7193), 406-409. (2008)

Ponsford J. Factors contributing to outcome following traumatic brain injury. *NeuroRehabilitation* 32, 803-815. (2013)

Portas CM, Rees G, Howseman AM, Josephs O, Turner R, Frith CD. A specific role for the thalamus in mediating the interaction of attention and arousal in humans. *J Neurosci* 18: 8979–8989. (1998)

Posner M. *Chronometric explorations of mind*. Lawrence Erlbaum. (1978)

Purpura KP, Schiff ND. The intralaminar nuclei: a role in visual awareness. *The Neuroscientist* 3, 8-15. (1997)

Purpura KP, Kalik SF, Schiff ND. Analysis of perisaccadic field potentials in the occipitotemporal pathway during active vision. *Journal of Neurophysiology* 90, 3455–3478. (2003)

Quinkert AW, Pfaff DW. Temporal patterns of deep brain stimulation generated with a true random number generator and the logistic equation: effects on CNS arousal in mice. *Behavioural brain research*, *229*(2), 349-358. (2012)

Riva-Posse P, Choi KS, Holtzheimer PE, McIntyre CC, Gross RE, Chaturvedi A, Mayberg HS. Defining critical white matter pathways mediating successful subcallosal cingulate deep brain stimulation for treatment-resistant depression. *Biological Psychiatry* 76(12), 963-969. (2014)

Rudolph M, Pelletier JG, Paré D, Destexhe A. Characterization of synaptic conductances and integrative properties during electrically induced EEG-activated states in neocortical neurons in vivo. *Journal of Neurophysiology* 94(4), 2805-2821. (2005)

Sanes JN, Donoghue JP. Oscillations in local field potentials of the primate motor cortex during voluntary movement. *Proceedings of the National Academy of Sciences* 90, 4470–4474. (1993)

Sarter M, Gehring WJ, Kozak R. More attention must be paid: the neurobiology of attentional effort. *Brain Research Reviews* 51, 145–160. (2006)

Schiff ND, Purpura KP. Towards a neurophysiological foundation for cognitive neuromodulation through deep brain stimulation. *Thalamus & Related Systems* 2(1), 55-69. (2002)

Schiff ND, Giacino JT, Kalmar K, Victor JD, Baker K, Gerber M, Fritz B, Eisenberg B, O'Connor J, Kobylarz EJ, Farris S, Machado A, McCagg C, Plum F, Fins JJ, Rezai, AR. Behavioural improvements with thalamic stimulation after severe traumatic brain injury. *Nature* 448, 600–603. (2007)

Schiff ND. Central thalamic contributions to arousal regulation and neurological disorders of consciousness. *Annals of the New York Academy of Sciences* 1129, 105–118. (2008)

Schiff ND. Moving toward a generalizable application of central thalamic deep brain stimulation for support of forebrain arousal regulation in the severely injured brain. *Annals of the New York Academy of Sciences* 1265(1), 56-68. (2012)

Schiff ND, Shah SA, Hudson AE, Nauvel T, Kalik SF, Purpura KP. Gating of attentional effort through the central thalamus. *Journal of Neurophysiology* 109(4), 1152-1163. (2013)

Schlag-Rey M, Schlag J. Visuomotor functions of central thalamus in monkey. I. Unit activity related to spontaneous eye movements. *J Neurophysiol* 51: 1149–1174. (1984)

Schlag J, Schlag-Rey M. Visuomotor functions of central thalamus in monkey. II. Unit activity related to visual events, targeting, and fixation. *Journal of Neurophysiology* 51, 1175–1195. (1984)

Shah SA, Baker JL, Ryou JW, Purpura KP, Schiff, ND Modulation of arousal regulation with central thalamic deep brain stimulation. In *Conf Proc IEEE Eng Med Biol Soc*, pp. 3314-3317. (2009)

Shirvalkar P, Seth M, Schiff ND, Herrera DG. Cognitive enhancement with central thalamic electrical stimulation. *Proceedings of the National Academy of Sciences* 103, 17007-17012. (2006)

Skinner JE, Yingling CD. Reconsideration of the cerebral mechanisms underlying selective attention and slow potential shifts. *Attention, voluntary contraction and event-related cerebral potentials. Progress in clinical neurophysiology*, *1*, 30-69. (1977)

Smith AC, Shah SA, Hudson AE, Purpura, KP, Victor JD, Brown EN, Schiff ND. A Bayesian statistical analysis of behavioral facilitation associated with deep brain stimulation. *Journal of Neuroscience Methods* 183, 267–276. (2009)

Stanslaski S, Afshar P, Cong P, Giftakis J, Stypulkowski P, Carlson D, Denison T. Design and validation of a fully implantable, chronic, closed-loop neuromodulation device with concurrent sensing and stimulation. *IEEE Transactions on Neural Systems and Rehabilitation Engineering* 20(4), 410-421. (2012)

Steinborn MB, Langner R. Arousal modulates temporal preparation under increased time uncertainty: evidence from higher-order sequential foreperiod effects. *Acta psychologica* 139, 65–76. (2012)

Steriade M, Llinás RR. The functional states of the thalamus and the associated neuronal interplay. *Physiol rev* 68.3: 649-742. (1988)

Steriade M, Pare D, Parent A, Smith Y. Projections of cholinergic and non-cholinergic neurons of the brainstem core to relay and associational thalamic nuclei in the cat and macaque monkey. *Neuroscience*, *25*(1), pp.47-67. (1988)

Steriade M, Dossi RC, Pare D, Oakson G. Fast oscillations (20-40 Hz) in thalamocortical systems and their potentiation by mesopontine cholinergic nuclei in the cat. *Proceedings of the National Academy of Sciences*, *88*(10), 4396-4400. (1991)

Steriade M, Curro R, Contreras D. Electrophysiological properties of intralaminar thalamocortical cells discharging rhythmic (≈40 Hz) spike-bursts at ≈1000 Hz during waking and rapid eye movement sleep. *Neuroscience* 56.1: 1-9. (1993)

Steriade M, Contreras D, Amzica F, Timofeev I. Synchronization of fast (30-40 Hz) spontaneous oscillations in intrathalamic and thalamocortical networks. *The journal of Neuroscience* 16(8), 2788-2808. (1996)

Steriade, M, Amzica F, Contreras D. Synchronization of fast (30-40 Hz) spontaneous cortical rhythms during brain activation. *The Journal of Neuroscience* 16.1: 392-417. (1996)

Steriade M. Arousal - Revisiting the Reticular Activating System. *Science* 272(5259), 225-225. (1996)

Steriade M. Corticothalamic resonance, states of vigilance and mentation. *Neuroscience* 101: 243–276. (2000)

Steriade M, Timofeev I, Grenier F. Natural waking and sleep states: a view from inside neocortical neurons. Journal of Neurophysiology 85:1969 –1985. (2001)

Steriade M. Grouping of brain rhythms in corticothalamic systems. Neuroscience 137:1087–1106. (2006)

Stuss DT, Stethem LL, Hugenholtz H, Picton T, Pivik J, Richard MT. Reaction time after head injury: fatigue, divided and focused attention, and consistency of performance. *Journal of Neurology, Neurosurgery & Psychiatry*, *52*(6), 742-748. (1989)

Stuss DT, Pogue J, Buckle L, Bondar J. Characterization of stability of performance in patients with traumatic brain injury: variability and consistency on reaction time tests. *Neuropsychology*, *8*(3), 316. (1994)

Sutherland RJ. The dorsal diencephalic conduction system: a review of the anatomy and functions of the habenular complex. Neurosci. Biobehav. Rev. 6, 1–13. (1982)

Tabansky I, Quinkert AW, Rahman N, Muller SZ, Lofgren J, Rudling J, Pfaff DW. Temporally-patterned deep brain stimulation in a mouse model of multiple traumatic brain injury. *Behavioural brain research*, *273*, 123-132. (2014)

Talsky A, Pacione LR, Shaw T, Wasserman L, Lenny A, Verma A, Hurwitz G, Waxman R, Morgan A, Bhalerao S. Pharmacological interventions for traumatic brain injury. *British Columbia Medical Journal* 53, 26-31. (2010)

Thomson D. Multiple window method for obtaining improved spectrograms of signals. U.S. patent 6,351,729 B1. (2002)

Witham CL, Wang M, Baker SN. Cells in somatosensory areas show synchrony with beta oscillations in monkey motor cortex. *European Journal of Neuroscience* 26(9), 2677-2686. (2007)

Wyder MT, Massoglia DP, Stanford TR. Quantitative assessment of the timing and tuning of visual-related, saccade-related, and delay period activity in primate central thalamus. *Journal of Neurophysiology* 90: 2029–2052. (2003)

Wyder MT, Massoglia DP, Stanford TR. Contextual modulation of central thalamic delay-period activity: representation of visual and saccadic goals. *Journal of Neurophysiology* 91, 2628–2648. (2004)

Van der Werf YD, Witter MP, Uylings HBM, Jolles J. Neuropsychology of infarctions in the thalamus; a review, *Neuropsychologia* 38(5), 613–627. (2000)

Van der Werf YD, Scheltens P, Lindeboom J, Witter MP, Uylings H, Jolles J. Deficits of memory, executive functioning and attention following infarction in the thalamus; a study of 22 cases with localized lesions. *Neuropsychologia* 41(10), 1330-1344. (2003)

Varazzani C, San-Galli A, Gilardeau S, Bouret S. Noradrenaline and dopamine neurons in the reward/effort trade-off: a direct electrophysiological comparison in behaving monkeys. *The Journal of Neuroscience*, *35*(20), pp.7866-7877. (2015)

Verhoef BE, Vogels R, Janssen P. Synchronization between the end stages of the dorsal and the ventral visual stream. *Journal of Neurophysiology* 105(5), 2030-42. (2011)

Viola P, Wells WMI. Alignment by maximization of mutual information. *International Journal of Computer Vision*, 24, 137–154. (1997)

Vitek JL. Deep brain stimulation: how does it work? *Cleveland Clinic Journal of Medicine* 75 (Suppl. 2), S59. (2008)

Yerkes RM, Dodson JD. The relation of strength of stimulus to rapidity of habit-formation. J. Comp. Neurol. Psychol. 18, 459–482. (1908)

Zhang Y, Chen Y, Bressler SL, Ding M. Response preparation and inhibition: the role of the cortical sensorimotor beta rhythm. *Neuroscience* 156(1), 238-246. (2008)

Ziino C, Ponsford J. Selective attention deficits and subjective fatigue following traumatic brain injury. *Neuropsychology*, *20*(3), 383. (2006)

Figure Captions

Fig. 1. The animal's typical behavioral performance of the vigilance task during experimental sessions without central thalamic deep brain stimulation. When motivated to work for juice rewards, both animals typically performed until satiated and then ceased to work. ***A:*** Structure of the vigilance task. To perform correctly, the animal had to maintain stable fixation (2 degree visual angle) on the displayed target (red/black dartboard) that would undergo contrast reversal, at 10Hz, during stable fixation. The contrast reversal indicated the start of the variable delay period that would last 1.5-4.5 seconds and ended when the color of the target switched from red/black to green/black, 'GO' cue, instructing the animal to touch an infrared switch for juice reward. ***B:*** Native behavioral performance of NHP1 during the vigilance task. The performance estimate is shown as a smoothly varying blue line (Smith et al. 2009) and reaction times of correctly performed trials are plotted in black. The red line indicates the cumulative number of incorrect trials. Periods of slow rolling eye-movements, eye closure and a presumed increase in drowsiness co-occurred with marked increases in the power of low frequency oscillatory activity (4-8Hz) recorded in frontal and midline ECoG electrodes (see *Methods*) and are marked in

green along the zero performance line. Mean delay period was 2.2 seconds and average performance in this session was 60% correct (660 of 1100 trials). Trial number and total time on task are indicated. ***C:*** Same as in *B* but for NHP2. Mean delay period was 4.2 seconds and average performance during this session was 61% correct (673/1100 trials). Note the trending decrease in average performance and increased variance in reaction times following trial 600 in both animals, corresponding to ~43 and 68 minutes time on task respectively. Periods of eye closure and presumed increased drowsiness occurred frequently in the later half of most experimental sessions. These trends are consistent with performance changes observed in additional animals performing the identical vigilance task (Smith et al. 2009; Shah et al. 2009) and in humans performing similar tasks continuously over extend periods of time (Paus et al., 1997).

Fig. 2. Central thalamic deep brain stimulation markedly effects the animals performance on the vigilance task. ***A:*** The performance estimate of NHP1 on repeated trials of the vigilance task is shown as a smoothly varying black line. Performance was estimated from correct and incorrect trial completion (Smith et al. 2009) and only the first 1600 (154 minutes) of 2500 (230 minutes) trials in this example session are shown. Periods of continuous fsCT-DBS are colored according to significant behavioral facilitation (green) and non-significant change in behavioral performance (gray) based on the LOR value ($p<0.05$) for each period. The same anode-cathode configuration, right caudal cathode contact 0, rostral anode contact 0 and stimulation amplitude of 1.75mA was used in all periods shown. Two segments of contiguous trials labeled ‘induction’ and ‘control’ represent phases of behavioral change that occurred during the ON and OFF fsCT-DBS paradigm. Note the general decline in average performance during the ‘induction’ phase, and then the eventual ‘control’ of performance, established after trial 700 (73 minutes). ***B:*** Reaction times of correct trials occurring within fsCT-DBS ON periods are colored as in *B* and black during OFF periods. ***C:*** Same as in *B*, but for NHP2. The same anode-cathode configuration, bilateral caudal cathode contact 4, rostral anode contact 4 was used throughout, however significant facilitation (green) of performance was observed when stimulation amplitudes ranged from 0.5 to 1.0mA and consistent behavioral suppression (red) was observed when stimulation amplitudes ranged from 1.5 to 3.0mA. A similar decline in average performance is seen during the ‘induction’ phase and with a lesser degree of ‘control’ established after trial 700 (66 minutes) to trial 1600 (147 minutes). ***D:*** Same as in *C*, but for NHP2.

1654 **Fig. 3.** The relationship between the amplitude of central thalamic deep brain stimulation and
1655 the animal's performance on the vigilance task. ***A:*** The performance estimate of NHP1 on the
1656 vigilance task is shown as a smoothly varying black line (Smith et al. 2009). Periods of
1657 continuous high frequency fsCT-DBS are colored according to the significance of the LOR value
1658 ($p<0.05$) for each period; behavioral facilitation in green, behavioral suppression in red and gray
1659 for no significant change in performance. Stimulation amplitudes, ranging 0.75 to 3.0 mA, are
1660 noted above each fsCT-DBS period along with the LOR value. The same anode-cathode
1661 configuration, right caudal cathode contact 0, rostral anode contact 0 was used throughout.
1662 Note that once 'control' of performance was established after trial 500 (57 minutes), stimulation
1663 amplitudes between 1.25 and 2.5 robustly facilitated performance while amplitudes below and
1664 above this range had little or no effect on performance. ***B:*** Reaction times occurring within fsCT-
1665 DBS ON periods are colored as in *A* and black during OFF periods. ***C:*** Same as in *A*, but for
1666 NHP2. In this session, fsCT-DBS stimulation amplitudes of 1.5mA and above significantly
1667 suppressed performance while amplitudes between 0.25 and 1.25mA had either no effect or
1668 modestly facilitated behavioral performance. The same anode-cathode configuration, left caudal
1669 cathode contact 4, rostral anode contact 4 was used throughout. ***D:*** Same as in *B*, but for
1670 NHP2. In both animals stimulation amplitude markedly influenced behavioral performance
1671 where low and high amplitudes had either no effect or significantly suppressed performance
1672 (LOR, $p<0.05$) and where amplitudes in-between facilitated performance, demonstrating an
1673 inverted-U relationship between stimulation amplitude and performance (Yerkes and Dodson
1674 1908; Mair et al. 2008).
1675

1676 **Fig. 4.** Summary of central thalamic deep brain stimulation's influence on the animals
1677 behavioral performance. Here, the odds ratio is the probability of the animal performing a
1678 correct trial during DBS divided by the probability of performing a correct trial prior to DBS
1679 onset. The log of this ratio is the log odds ratio (LOR). Positive LOR values correspond to a
1680 greater probability of the animal performing a correct trial during DBS. ***A:*** Box plots of LOR
1681 values for all periods using field-shaping CT-DBS (fsCT-DBS) configurations (N=2187) grouped
1682 by amplitude of stimulation (0.25 to 3.0mA) for NHP1, recorded across 195 experimental
1683 sessions. The number of fsCT-DBS periods conducted for each amplitude is noted. The red line
1684 illustrates the fit of a 2nd order polynomial function to illustrate the inverted U relationship
1685 between performance and fsCT-DBS amplitude. ***B:*** Same as in *A*, but for all periods using
1686 standard CT-DBS configurations (N=274) in NHP1, recorded across 72 experimental sessions.
1687 ***C:*** Behavioral performance curves for DBS periods in *A* and *B*, each normalized to pre-DBS

performance levels, including ±95% CI. DBS periods with significant positive LOR values ($p<0.05$) using fsCT-DBS configurations (N=947) are shown in dark green and in light blue for standard CT-DBS configurations (N=36). DBS periods with non-significant LOR values ($p>0.05$) during fsCT-DBS configurations (N=1091) are shown in black and in gray for standard CT-DBS configurations (N=220). DBS periods with significant negative LOR values ($p<0.05$) are not shown. The gray shaded region represents the DBS ON period. ***D:*** Same as in *A*, but for NHP2, fsCT-DBS configurations (N=447) recorded across 46 experimental sessions. ***E:*** Same as in *B*, but for NHP2, standard CT-DBS configurations (N=214) recorded across 21 experimental sessions. ***F:*** Same as in C, but for NHP2.

Fig. 5. Graded and task related modulation of frontostriatal LFP activity during the vigilance task is markedly enhanced during fsCT-DBS. ***A:*** Average power spectra of 1236 frontal-striatal LFP signals recorded in NHP1 during fsCT-DBS OFF periods and restricted to 1 second prior to the delay period (between seconds 1 and 2 of the trial, see Fig. 1*A*) of both Correct (shown in red, 14,258 trials) and InCorrect (shown in blue, 39,836 trials) trials. Black points along the bottom of the frequency axis indicate significant difference between the two power spectra (two-group test, $p<0.05$ (Bokil et al. 2007) and false discovery rate, $p<0.05$ (Benjamini and Hochberg 1995)). ***B:*** Spectrogram combining frontal and striatal LFP activity recorded during the performance of the vigilance task by NHP1. A total of 68 sessions and 1005 LFP recording sites are included. The 2-D plot of the spectrogram was averaged across 12,310 correct trials (153,425 spectra) recorded during OFF fsCT-DBS periods. Time is on the x-axis; frequency is on the y-axis. Decibel power is color-coded on a log scale. The first vertical line at 1 second indicates the appearance of the fixation target (red/black dartboard) on the video monitor (Fig. 1*A*). The second vertical line at 2 seconds indicates the start of the delay period. The final vertical line at ~ 4.2 seconds indicates the average endpoint of the variable delay period. ***C:*** 2-D plot of the spectrogram averaged across 13,354 Correct trials (142,696 spectra) recorded during fsCT-DBS ON periods (N=893). Field shaping CT-DBS was established with cathode(s) set on the caudal DBS lead contacts 0, 1 and/or 2 and anodes(s) set on the rostral DBS lead contacts 0, 1 and/or 2. Only stimulation frequencies of 150, 175, 200 and 225Hz are included and the stimulation amplitude ranged from 0.75 to 2.5mA. ***D:*** 2-D plot of the average spectral difference, i.e. the difference between the average OFF and ON fsCT-DBS spectra shown in *B* and *C,* respectively. ***E:*** Same as in A, but for 60 frontal LFP recording sites in NHP2, 4,275 Correct trials (shown in red) and 4,168 InCorrect trials (shown in blue) during fsCT-DBS OFF periods. ***F:*** Spectrograms of population frontal LFP activity recorded during the performance of

the vigilance task by NHP2. A total of 15 sessions, 153 fsCT-DBS periods and 60 LFP recording sites are included. The 2-D plot of the spectrogram was averaged across 4,122 Correct trials (16,385 spectra) recorded during OFF fsCT-DBS periods. Time is on the x-axis; frequency is on the y-axis. Decibel power is color-coded on a log scale. The last vertical line at 4.8 seconds indicates the average endpoint of the variable delay period. ***G:*** 2-D plot of the spectrogram averaged across 1,826 Correct trials (7,478 spectra) recorded during fsCT-DBS ON periods. Field shaping CT-DBS was established with cathode(s) set on the caudal DBS lead contacts 3, 4 and/or 5 and anodes(s) set on the rostral DBS lead contacts 3, 4 and/or 5. Only stimulation frequencies of 150, 175, 200 and 225Hz are included and the stimulation amplitudes ranged from 0.5 to 1.5mA. ***H:*** 2-D plot of the average spectral difference, i.e. the difference between the average OFF and ON fsCT-DBS spectra shown in *F* and G*,* respectively.

Fig. 6. Field shaping CT-DBS markedly shifts power spectra of local field potentials measured in frontal and striatal regions. ***A:*** A bandpass filtered, 10-40Hz, LFP recorded from the frontal cortex of NHP1. The onset of high frequency (200Hz) 2.0mA fsCT-DBS is marked by the red line at 0 seconds. ***B:*** Same as in A, but for NHP2. fsCT-DBS amplitude was 1.5mA. ***C:*** Average power spectra of an LFP recorded from the frontal cortex of NHP1, restricted to the delay period of correctly performed trials, 481 fsCT-DBS ON trials and 886 fsCT-DBS OFF trials, averaged across 22 fsCT-DBS periods from one experimental session. Black points along the bottom of the frequency axis indicate significant difference between power spectra (two-group test, $p<0.05$ (Bokil et al. 2007), false discovery rate, $p<0.05$ (Benjamini and Hochberg 1995)). ***D:*** Left-side is average LFP power and right-side is average Z-score of LFP power (*see Methods*) concatenated over 10 trials prior to fsCT-DBS onset, indicated by dashed vertical line at trial 0, and 15 trials during fsCT-DBS. The average 2-D spectrograms include LFP activity recorded from 2577 frontal and striatal sites, aggregated over 1423 fsCT-DBS periods conducted in 154 experimental sessions in NHP1. Stimulation amplitudes ranged from 0.75 to 2.5mA and frequencies of 150, 175, 200 and 225Hz. ***E:*** Average Z-score's of LFP power spectra shown in *D,* but during the delay period of Correct trials during fsCT-DBS ON periods (19,349 trials, 283,423 spectra), relative to delay period activity of Correct trials during fsCT-DBS OFF periods (19,320 trials, 298,216 spectra), including ±95% CI. The z-score power spectra for each LFP site was corrected for unequal trial numbers between the two conditions (two-group test, $p<0.05$) and corrected for multiple comparisons across the frequencies in the spectra (false discovery rate, $p<0.05$) prior to averaging. Z-scores are grouped according to a range of stimulation amplitudes, 0.75-1.25, 1.50-1.75 and 2.0-2.5mA. ***F:*** Same as in C, but for NHP2.

338 fsCT-DBS ON trials and 577 fsCT-DBS OFF trials, averaged across 17 fsCT-DBS periods from one experimental session. ***G:*** Same as in *D*, but for 60 frontal LFP sites recorded in NHP2. The average plots include LFP activity aggregated over 143 fsCT-DBS periods across 15 sessions. Stimulation amplitudes ranged from 0.75 to 2.5mA and frequencies of 150, 175, 200 and 225Hz. ***H:*** Same as in *E*, but for 60 frontal LFP sites recorded in NHP2 and during the delay period of Correct trials during fsCT-DBS ON periods (1,581 trials, 6,130 spectra), relative to delay period activity Correct trials during fsCT-DBS OFF periods (4,122 trials, 6,385 spectra), including ±95% CI.

Fig. 7. Field shaping CT-DBS markedly shifts power spectra of local field potentials measured across various regions within the frontal cortex and dorsal striatum in NHP1. ***A:*** Left-side is average LFP power and right-side is average Z-score of LFP power (*see Methods*) concatenated over a series of 10 trials prior to fsCT-DBS onset, indicated by dashed vertical line at trial 0, and 15 trials during fsCT-DBS. LFP activity was recorded from 1305 sites within the frontal cortex and is aggregated over 1325 fsCT-DBS periods conducted in 144 experimental sessions. Stimulation amplitudes ranged from 0.75 to 2.5mA and stimulation frequencies of 150, 175, 200 and 225Hz were included. Field shaping CT-DBS was established with cathode(s) set on the caudal DBS lead contacts 0, 1 and/or 2 and anodes(s) set on the rostral DBS lead contacts 0, 1 and/or 2. ***B:*** Average Z-score of the LFP power spectra shown in *A*, but during the delay period of Correct trials during fsCT-DBS ON periods, relative to the delay period activity of Correct trials recorded during fsCT-DBS OFF periods, including ±95% CI. The Z-score power spectra for each LFP site was corrected for unequal trial numbers between the two conditions (two-group test, $p<0.05$) and corrected for multiple comparisons across the frequencies in the spectra (false discovery rate, $p<0.05$) prior to averaging. Z-scores are grouped according to three sets of stimulation amplitudes, 0.75-1.25, 1.50-1.75 and 2.0-2.5mA. ***C:*** Same as in *A*, but for LFP activity recorded from 1024 sites within the dorsal striatum and aggregated over 1009 fsCT-DBS periods conducted in 121 experimental sessions. ***D:*** Same as in *B*, but for the LFP power spectra shown in *C* that was recorded within the dorsal striatum.

Fig. 8. The polarity of fsCT-DBS strongly affects NHP1's behavioral performance and frontalstriatal physiology. ***A:*** Sagittal view of the biophysical model of the right thalamus of NHP1. DBS lead locations were confirmed through histological reconstruction (Fig. 10*B*). The red structure represents the central lateral (CL) and paracentral (Pc) nuclei and the magenta structure represents the central median (CM) and parafascicular (Pf) complex. The purple

1790 structure represents the thalamic reticular nucleus (TRN). The caudal DBS lead ('C') is shown
1791 with blue contacts and the rostral DBS lead ('R') is shown with green contacts. Three single
1792 anode-cathode bipolar pairs are illustrated, where active contacts are placed between the two
1793 leads (C1 and C2) or within the same lead (C3). Inter-lead configurations are field-shaping CT-
1794 DBS (fsCT-DBS) and intra-lead configurations are standard CT-DBS. Stimulation between
1795 contacts 0, 1 and 2 on both leads, using fsCT-DBS configurations (C1, C4 and C5), produced
1796 robust and reliable behavioral effects and frontostriatal recruitment in NHP1. Effective
1797 stimulation amplitudes ranged from 0.75 to 2.5mA. ***B:*** Average performance change during
1798 fsCT-DBS and standard CT-DBS, ±95% CI, for the single anode-cathode configurations, C1, C2
1799 and C3 shown in *A*. Each configuration is color coded, red for C1, blue for C2 and green for C3.
1800 ***C:*** Average Z-score's of LFP power spectra recorded during the delay period of Correct trials,
1801 for each single anode-cathode configurations C1-C3 shown in *B*. Z-scores of the power spectra
1802 were corrected for unequal trial numbers (two-group test, $p<0.05$) and the false discovery rate
1803 ($p<0.05$). Frequencies of 150, 175, 200 and 225Hz are included and amplitudes ranged from
1804 0.75 to 2.5mA. Same color code as in *B*. ***D:*** Same as in *B*, but for all dual anode-cathode bipolar
1805 pairs, where multiple active contacts are placed on the two leads (C4 and C5) or on multiple
1806 contacts within the two leads (C6). ***E:*** Same as in *C*, but for all dual anode-cathode
1807 combinations, C4, C5 and C6.
1808
1809 **Fig. 9.** Biophysical models of axonal activation during field-shaping CT-DBS producing
1810 behavioral facilitation and frontalstriatal activation. ***A:*** Posterior view of the transparent 3D mesh
1811 surface model (white) of NHP1's right thalamus used for surgical planning. Solid colored 3D
1812 models of the central thalamic nuclei, rostral CL/Pc (red) and caudal CM/Pf (magenta), and the
1813 TRN (purple) are shown. A 6-contact DBS lead is positioned to optimally target the 'wing' of the
1814 rostral CL/Pc nuclei and DTTm fiber tracts. A pre-operative parasagittal MR image is shown for
1815 reference, CC - Splenium of the Corpus Callosum. ***B:*** Model of the 6-contact DBS lead and the
1816 voltage contour generated with the electric field model (Butson et al. 2011, see *Methods*) of
1817 standard intra-lead bipolar stimulation using a 1.5mA pulse, with the cathode is placed on
1818 contact 0 and the anode placed on contact 1. A schematic of a straight axon located at one grid
1819 node location and oriented in one of the 13 directions modeled. The red colored segment of the
1820 axon represents locations activated during stimulation (see *Methods*). ***C:*** Lateral view of central
1821 thalamic nuclei and two DBS leads located in the right thalamus of NHP1. Individual grid nodes,
1822 shown in yellow, represent the modeled axon nodes, derived from DTI (Adluru et al. 2012), that
1823 are activated during all fsCT-DBS configurations (Fig. 8, C1 and C4) that resulted in behavioral

1824 facilitation and frontostriatal activation. ***D:*** Posterior view of *C.* Shown in cyan are the modeled
1825 axonal nodes activated during all fsCT-DBS configurations (Fig. 8, C1 and C4) subtracted from
1826 all other fsCT-DBS and standard CT-DBS configurations (Fig. 8, C2, C3, C5 and C6) to illustrate
1827 the differential activation when cathode(s) were restricted to contacts 0, 1, and 2 on the caudal
1828 DBS lead and the charge balancing anode(s) were restricted to the rostral DBS lead. The white
1829 oval represents the approximate location of the DTTm (Edlow et al. 2012), a diffused fiber
1830 pathway containing principle CT fibers and en passant fibers originating from the ARAS that
1831 terminate within the CT and TRN as illustrated in Fig. 10*A*. ***E:*** Same as in *C*, but for NHP2. ***F:***
1832 Dorsal view of *D*. ***G:*** Dorsal view of *E*. Note the differences in lead locations between the two
1833 animals and the positions relative to the DTTm, indicated by white ovals. A notable lack of
1834 axonal activation within the 'wing' of CL and paralaminar medial dorsal (MD) nucleus (not
1835 shown) is seen in NHP2, compared to NHP1. The biophysical models and histological
1836 reconstruction of the DBS leads (Fig. 10*B*,*C*), the caudal DBS lead in NHP2 was located
1837 ~2.0mm posterior and ~1.0mm medial relative to the caudal DBS lead in NHP1. In addition, the
1838 separation distance and angle between the rostral and caudal leads in the two animals differed
1839 by 0.6mm.
1840
1841 **Fig. 10.** Inferred mechanism of frontostriatal activation during field-shaping CT-DBS within the
1842 DTTm of the mammalian central thalamus. ***A:*** Axial view of the principle intra-thalamic fibers
1843 originating from CT nuclei, CL/Pc (red) and CM/Pf (magenta) that project within the TRN
1844 (purple) and diffusely within the anterior forebrain. Fiber tracts are superimposed on an axial T1
1845 coronal image at the level of the mid thalamus of a human (*ex vivo* 7T DTI), modified with
1846 permission (Edlow et al. 2012). Not shown are the ascending reticular activation system (ARAS)
1847 fibers of the medial dorsal tegmental tract (DTTm) that terminate within the central thalamic
1848 nuclei and TRN (Jones 2007; Edlow et al. 2012), instead these fibers are represented by
1849 straight yellow lines. The straight red and magenta lines represent known thalamocortical and
1850 thalamostriatal efferent projections originating from the principle cells of the CT to illustrate their
1851 hypothesized orthodromic activation by fsCT-DBS. The (**+**) symbols denote the proposed
1852 increase in afferent drive to known striatal and cortical circuits of the anterior forebrain. The
1853 location of the rostral anode and caudal cathode represents the polarity of the electric field that
1854 robustly and reliably modulated behavioral performance and frontostriatal physiology during
1855 fsCT-DBS. ***B:*** Photomicrograph of myelin and Nissl stained section of NHP1's right thalamus
1856 containing the caudal DBS lead. A semi-transparent schematic of the caudal DBS lead
1857 represents its approximate location and the red oval surrounding the distal three contacts, 0, 1

and 2, represents the estimated area of tissue influenced by fsCT-DBS, based on the biophysical modeling. Prominent central thalamic nuclear structures and a concentration of myelinated fibers are encircled by a black oval to represent the DTTm. ***C:*** Same as in *B* but for NHP2. Note the difference in location and orientation of the caudal DBS lead in NHP2 relative to the DTTm and central thalamic nuclei. Nuclei: CL - Central Lateral; CM - Central Medial; LHb - Lateral Habenula; MD - Medial Dorsal; MHb - Medial Habenula; Pf - Parafascicular; Pul - Pulvinar; PVG - Periventricular Gray; TRN - Thalamic Reticular Nucleus; VPM - Ventral Posterior Medial; VPL - Ventral Posterior Lateral. Fibers: ic - Internal Capsule; pcom - Posterior Commissure; sm - Stria Medullaris.

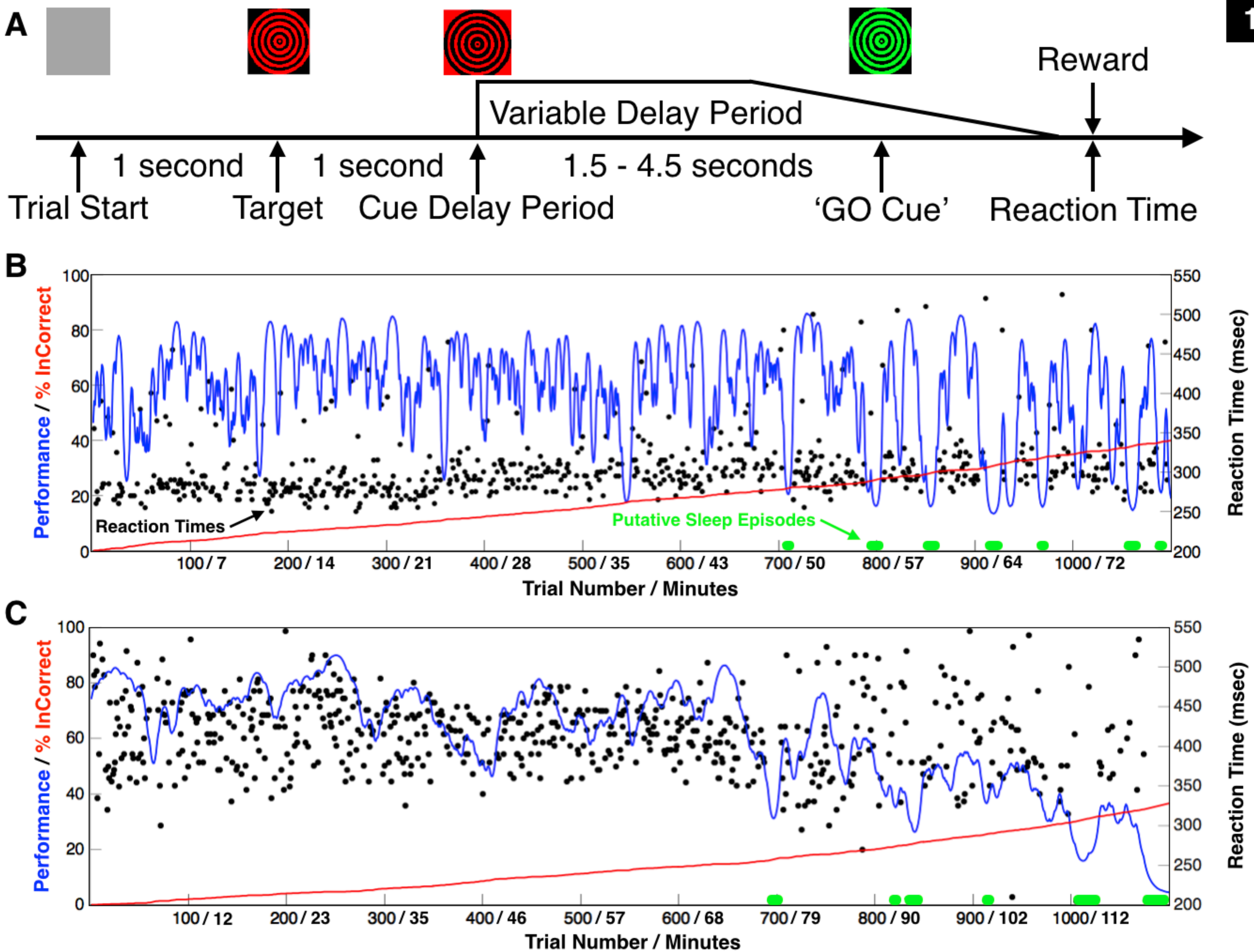
A
Reward
Variable Delay Period
1 second
1 second
1.5 - 4.5 seconds
Trial Start
Target
Cue Delay Period
'GO Cue'
Reaction Time
B
Performance / % InCorrect
Reaction Time (msec)
Reaction Times
Putative Sleep Episodes
100 / 7
200 / 14
300 / 21
400 / 28
500 / 35
600 / 43
700 / 50
800 / 57
900 / 64
1000 / 72
Trial Number / Minutes
C
Performance / % InCorrect
Reaction Time (msec)
100 / 12
200 / 23
300 / 35
400 / 46
500 / 57
600 / 68
700 / 79
800 / 90
900 / 102
1000/ 112
Trial Number / Minutes

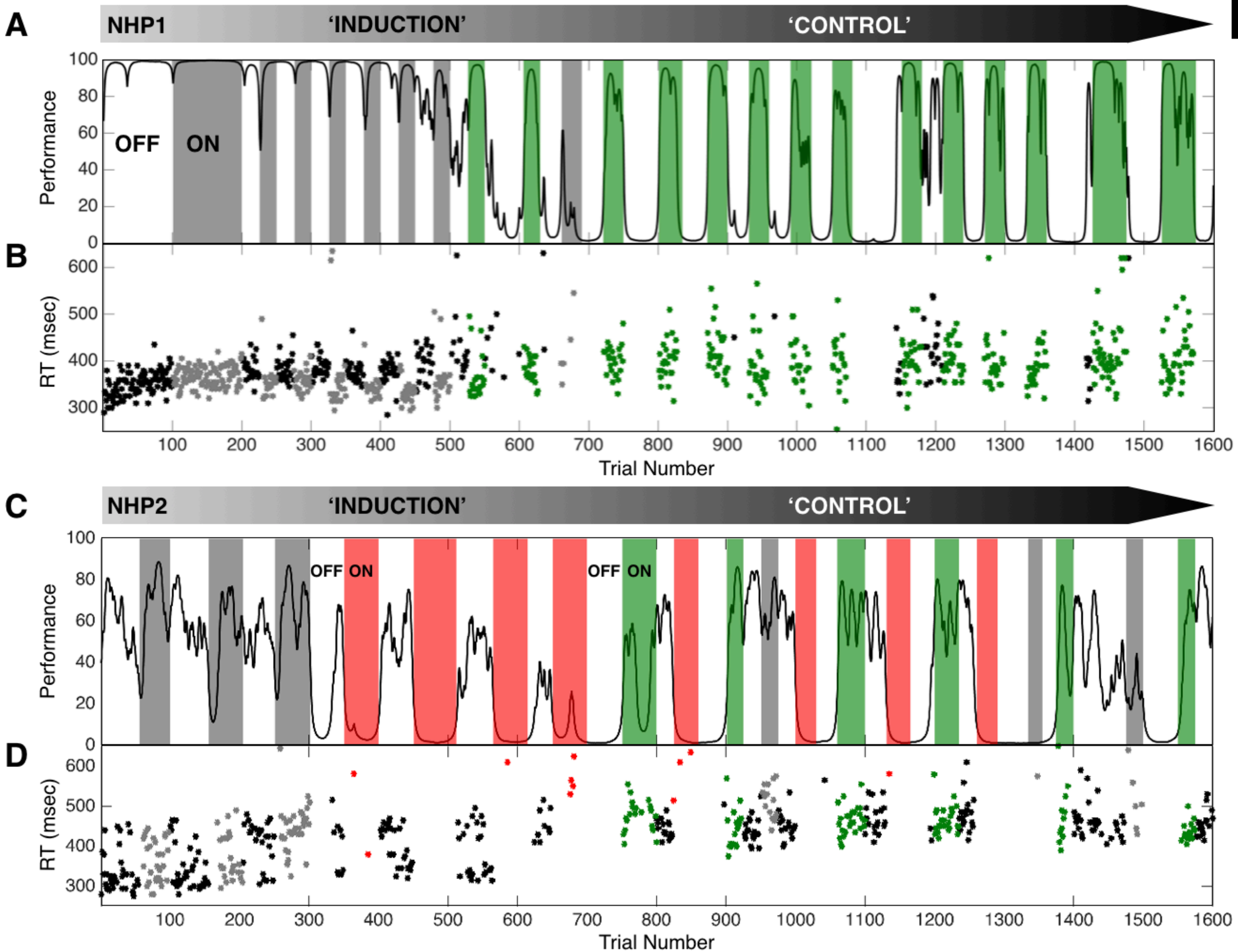
A
NHP1
'INDUCTION'
'CONTROL'
Performance
OFF
ON
B
RT (msec)
Trial Number
C
NHP2
'INDUCTION'
'CONTROL'
Performance
OFF
ON
OFF
ON
D
RT (msec)
Trial Number

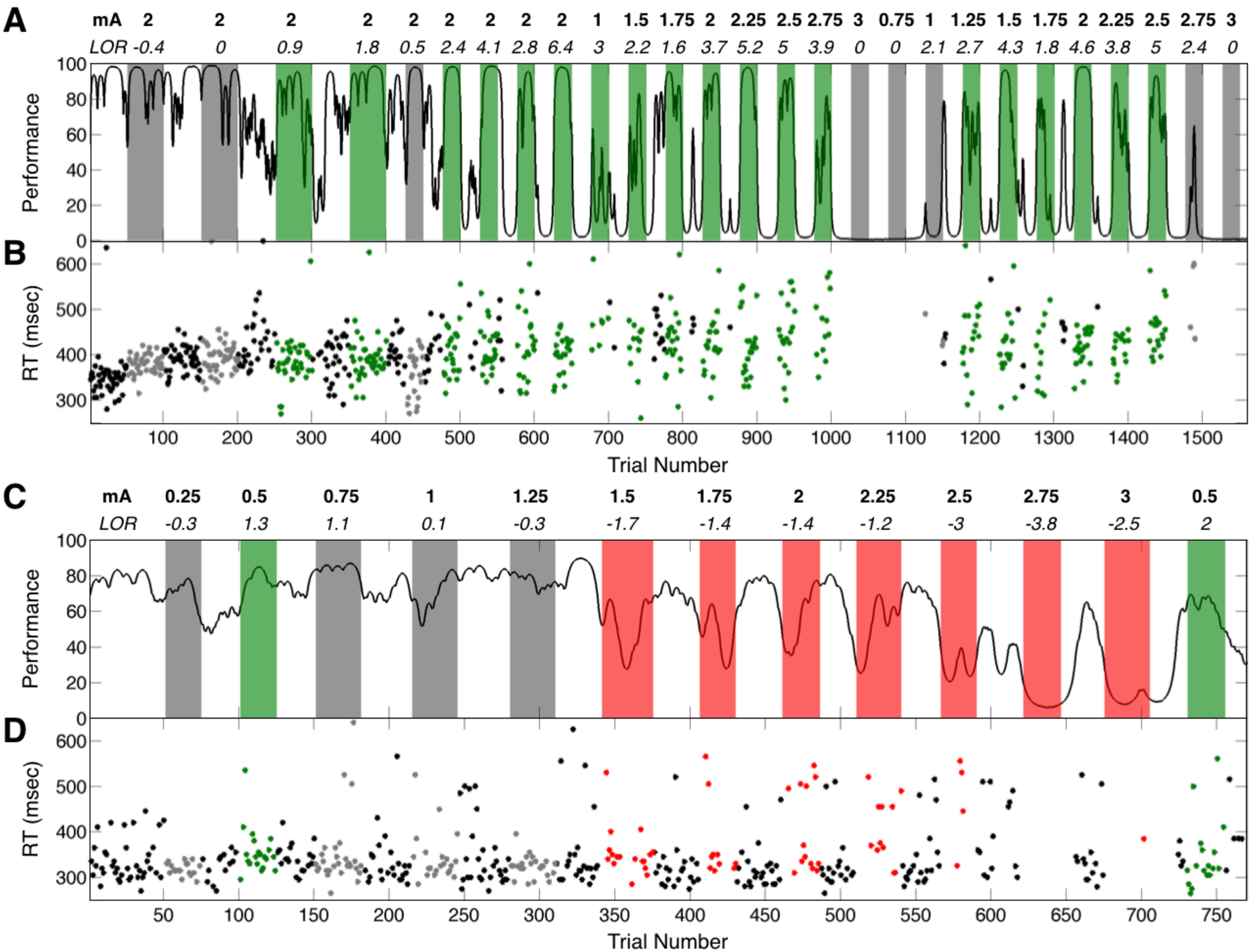
A
mA 2 2 2 2 2 2 2 2 2 1 1.5 1.75 2 2.25 2.5 2.75 3 0.75 1 1.25 1.5 1.75 2 2.25 2.5 2.75 3
LOR -0.4 0 0.9 1.8 0.5 2.4 4.1 2.8 6.4 3 2.2 1.6 3.7 5.2 5 3.9 0 0 2.1 2.7 4.3 1.8 4.6 3.8 5 2.4 0
Performance
B
RT (msec)
Trial Number
C
mA 0.25 0.5 0.75 1 1.25 1.5 1.75 2 2.25 2.5 2.75 3 0.5
LOR -0.3 1.3 1.1 0.1 -0.3 -1.7 -1.4 -1.4 -1.2 -3 -3.8 -2.5 2
Performance
D
RT (msec)
Trial Number

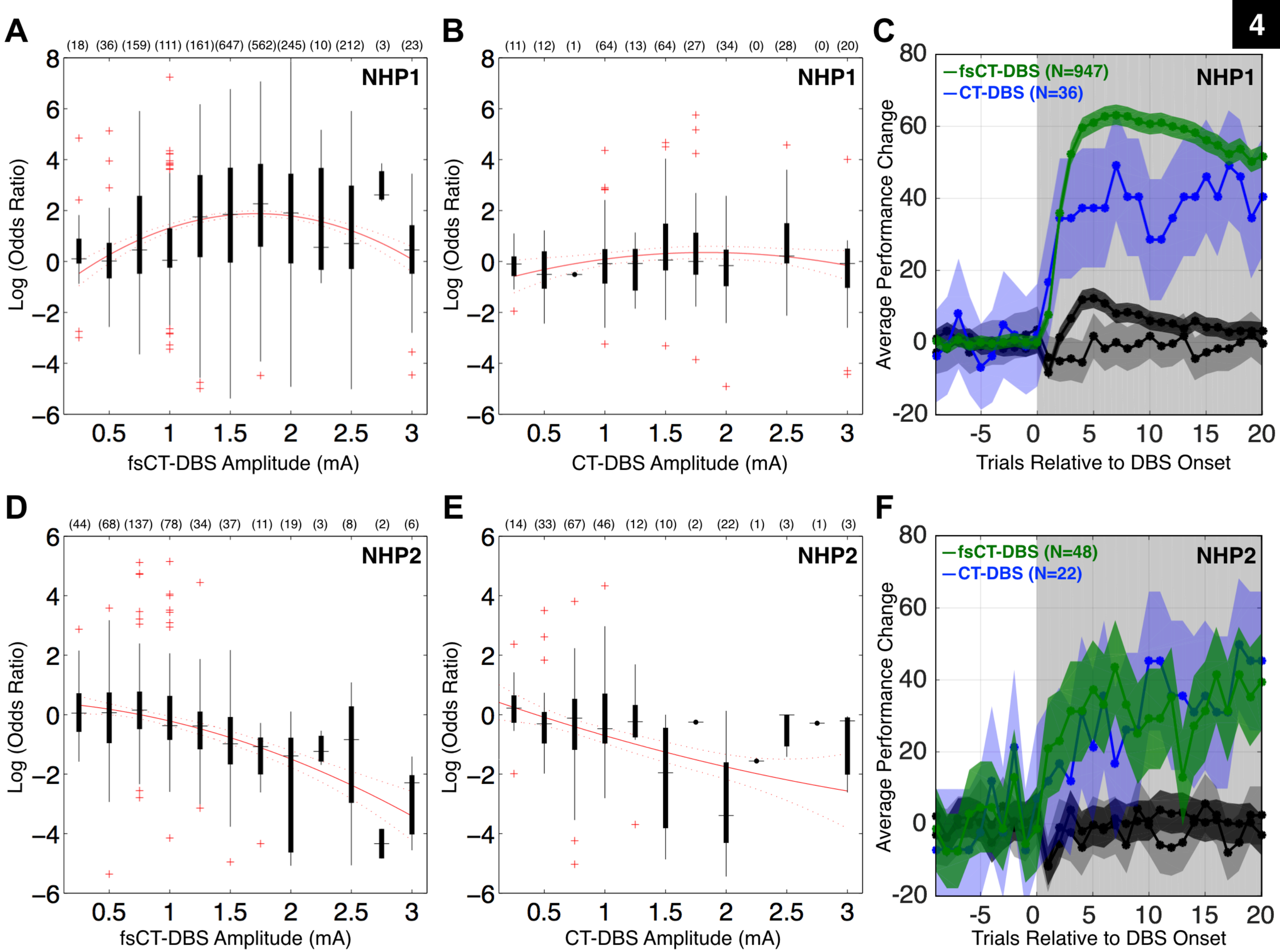
A
(18) (36) (159) (111) (161)(647) (562)(245) (10) (212) (3) (23)
NHP1
Log (Odds Ratio)
fsCT-DBS Amplitude (mA)
B
(11) (12) (1) (64) (13) (64) (27) (34) (0) (28) (0) (20)
NHP1
Log (Odds Ratio)
CT-DBS Amplitude (mA)
C
fsCT-DBS (N=947)
CT-DBS (N=36)
NHP1
Average Performance Change
Trials Relative to DBS Onset
D
(44) (68) (137) (78) (34) (37) (11) (19) (3) (8) (2) (6)
NHP2
Log (Odds Ratio)
fsCT-DBS Amplitude (mA)
E
(14) (33) (67) (46) (12) (10) (2) (22) (1) (3) (1) (3)
NHP2
Log (Odds Ratio)
CT-DBS Amplitude (mA)
F
fsCT-DBS (N=48)
CT-DBS (N=22)
NHP2
Average Performance Change
Trials Relative to DBS Onset

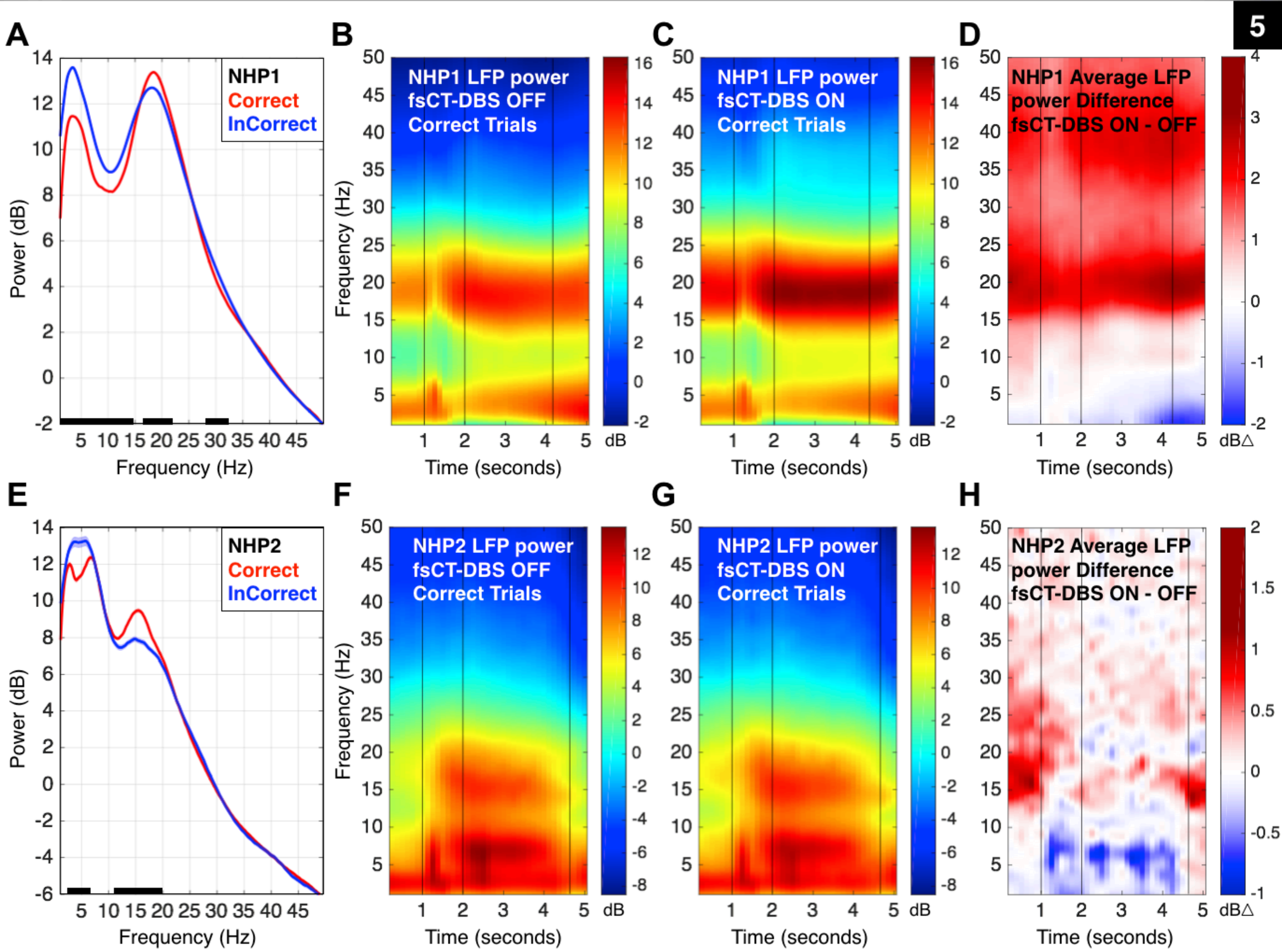
A
NHP1
Correct
InCorrect
Power (dB)
Frequency (Hz)
B
NHP1 LFP power
fsCT-DBS OFF
Correct Trials
Frequency (Hz)
Time (seconds)
dB
C
NHP1 LFP power
fsCT-DBS ON
Correct Trials
Time (seconds)
dB
D
NHP1 Average LFP
power Difference
fsCT-DBS ON - OFF
Time (seconds)
dB△
E
NHP2
Correct
InCorrect
Power (dB)
Frequency (Hz)
F
NHP2 LFP power
fsCT-DBS OFF
Correct Trials
Frequency (Hz)
Time (seconds)
dB
G
NHP2 LFP power
fsCT-DBS ON
Correct Trials
Time (seconds)
dB
H
NHP2 Average LFP
power Difference
fsCT-DBS ON - OFF
Time (seconds)
dB△

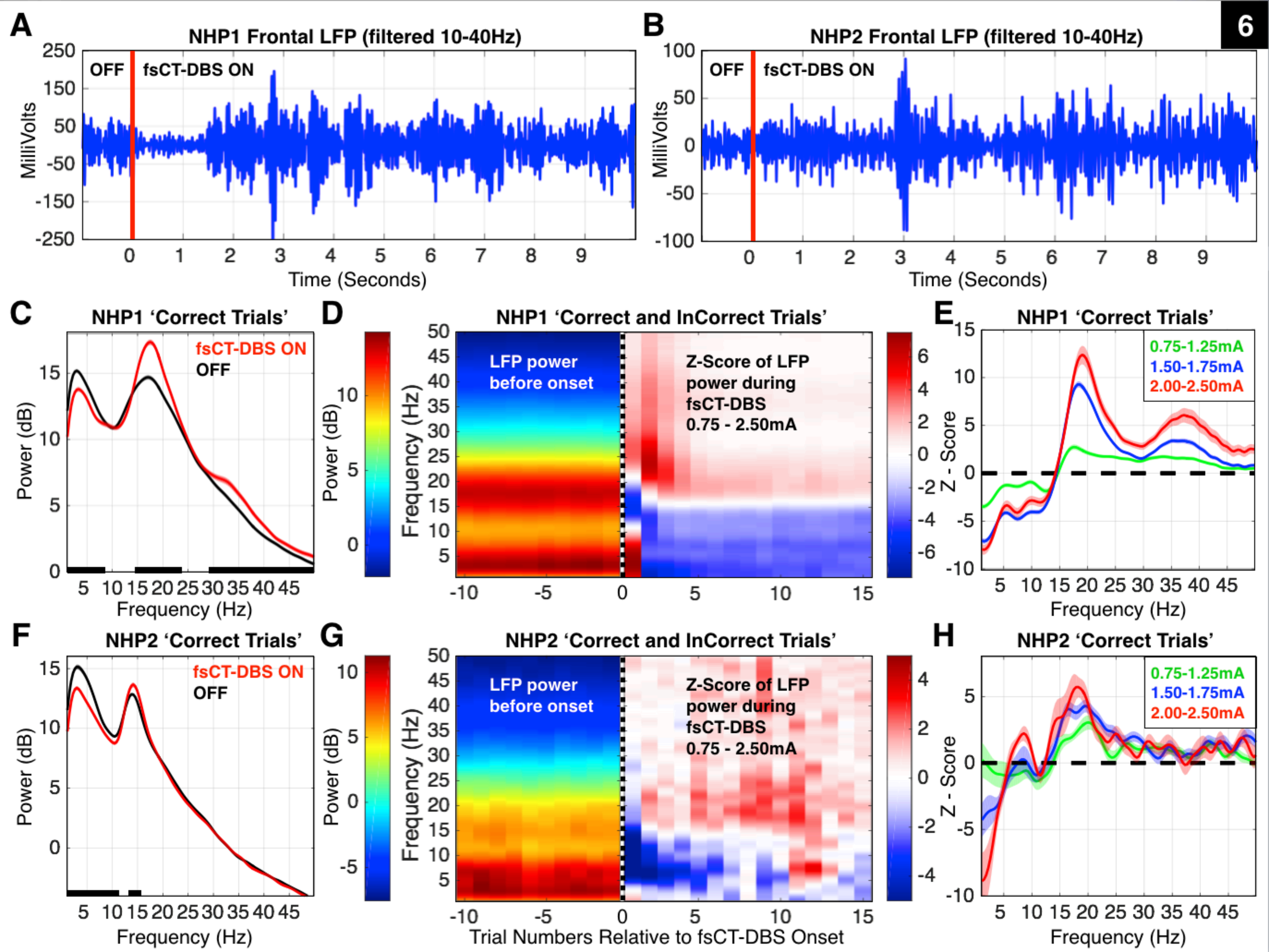
A
NHP1 Frontal LFP (filtered 10-40Hz)
OFF
fsCT-DBS ON
MilliVolts
Time (Seconds)
B
NHP2 Frontal LFP (filtered 10-40Hz)
OFF
fsCT-DBS ON
MilliVolts
Time (Seconds)
C
NHP1 'Correct Trials'
fsCT-DBS ON
OFF
Power (dB)
Frequency (Hz)
D
NHP1 'Correct and InCorrect Trials'
LFP power before onset
Z-Score of LFP power during fsCT-DBS 0.75 - 2.50mA
Power (dB)
Frequency (Hz)
E
NHP1 'Correct Trials'
0.75-1.25mA
1.50-1.75mA
2.00-2.50mA
Z - Score
Frequency (Hz)
F
NHP2 'Correct Trials'
fsCT-DBS ON
OFF
Power (dB)
Frequency (Hz)
G
NHP2 'Correct and InCorrect Trials'
LFP power before onset
Z-Score of LFP power during fsCT-DBS 0.75 - 2.50mA
Power (dB)
Frequency (Hz)
Trial Numbers Relative to fsCT-DBS Onset
H
NHP2 'Correct Trials'
0.75-1.25mA
1.50-1.75mA
2.00-2.50mA
Z - Score
Frequency (Hz)

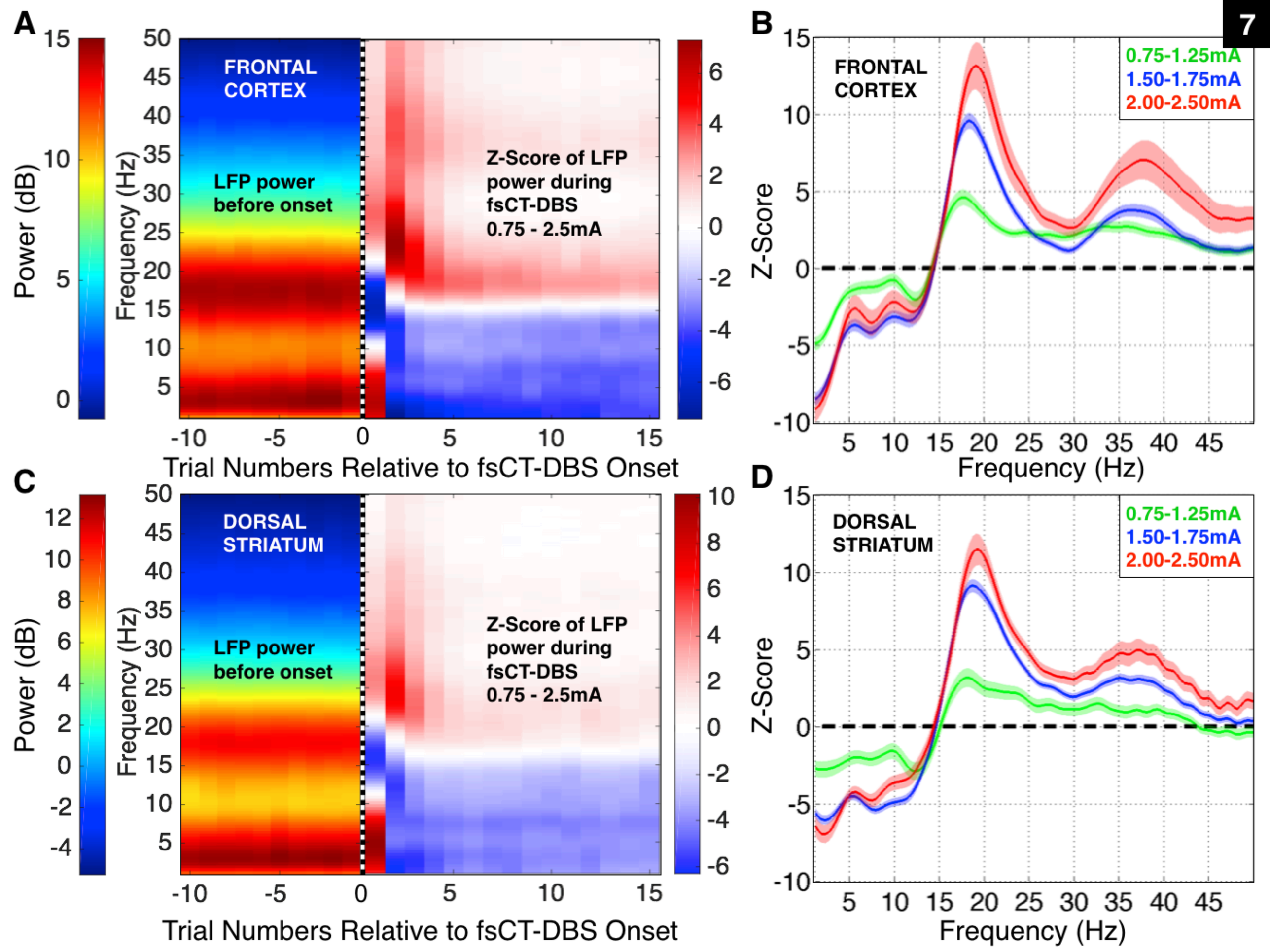
A
FRONTAL CORTEX
LFP power before onset
Z-Score of LFP power during fsCT-DBS 0.75 - 2.5mA
Power (dB)
Frequency (Hz)
Trial Numbers Relative to fsCT-DBS Onset
B
FRONTAL CORTEX
0.75-1.25mA
1.50-1.75mA
2.00-2.50mA
Z-Score
Frequency (Hz)
C
DORSAL STRIATUM
LFP power before onset
Z-Score of LFP power during fsCT-DBS 0.75 - 2.5mA
Power (dB)
Frequency (Hz)
Trial Numbers Relative to fsCT-DBS Onset
D
DORSAL STRIATUM
0.75-1.25mA
1.50-1.75mA
2.00-2.50mA
Z-Score
Frequency (Hz)

A

Anode-Cathode Configurations

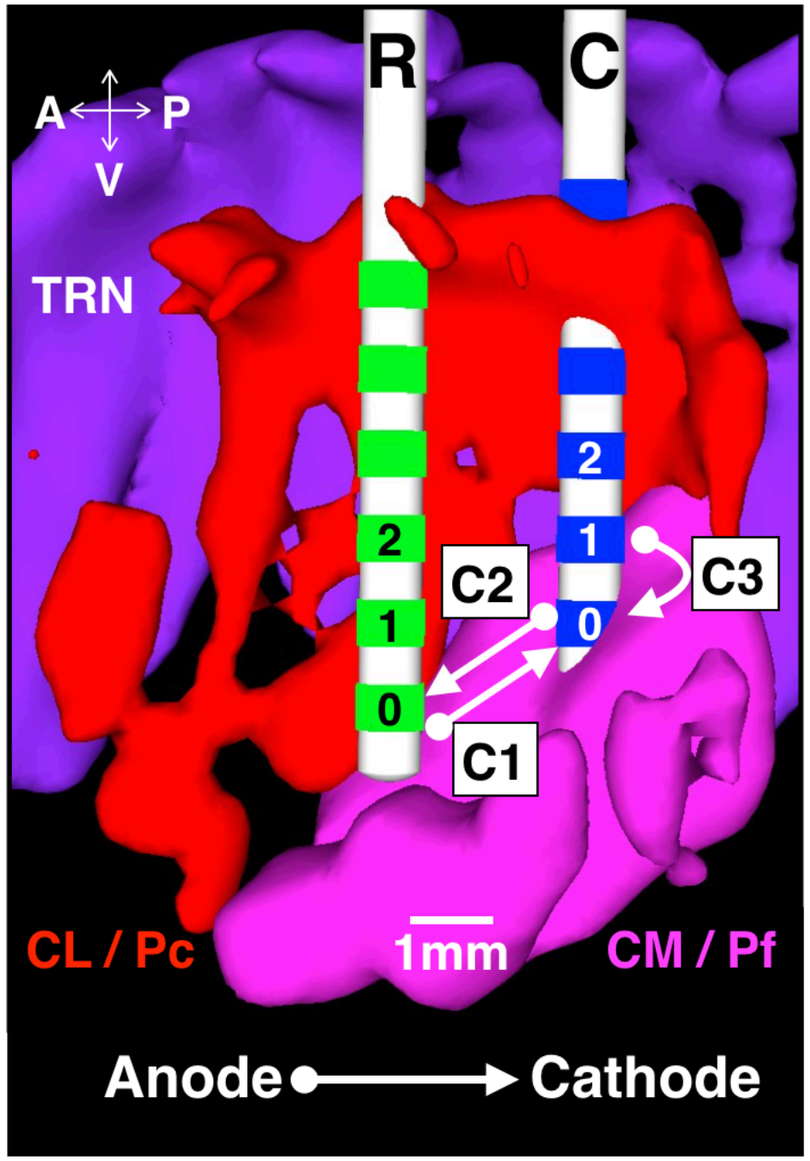

(*Dual* Anode-Cathode)

C4: Dual ***Inter*** Lead configurations (fsCT-DBS)
DBS Lead C = Two Cathodes
DBS Lead R = Two Anodes

C5: Dual ***Inter*** Lead configurations (fsCT-DBS)
DBS Lead C = Two Anodes
DBS Lead R = Two Cathodes

C6: Dual ***Intra*** Lead configurations (CT-DBS)
Pairs of Cathodes and Anodes
placed on the same DBS lead

B

Behavioral Effects

(*Single* Anode-Cathode)

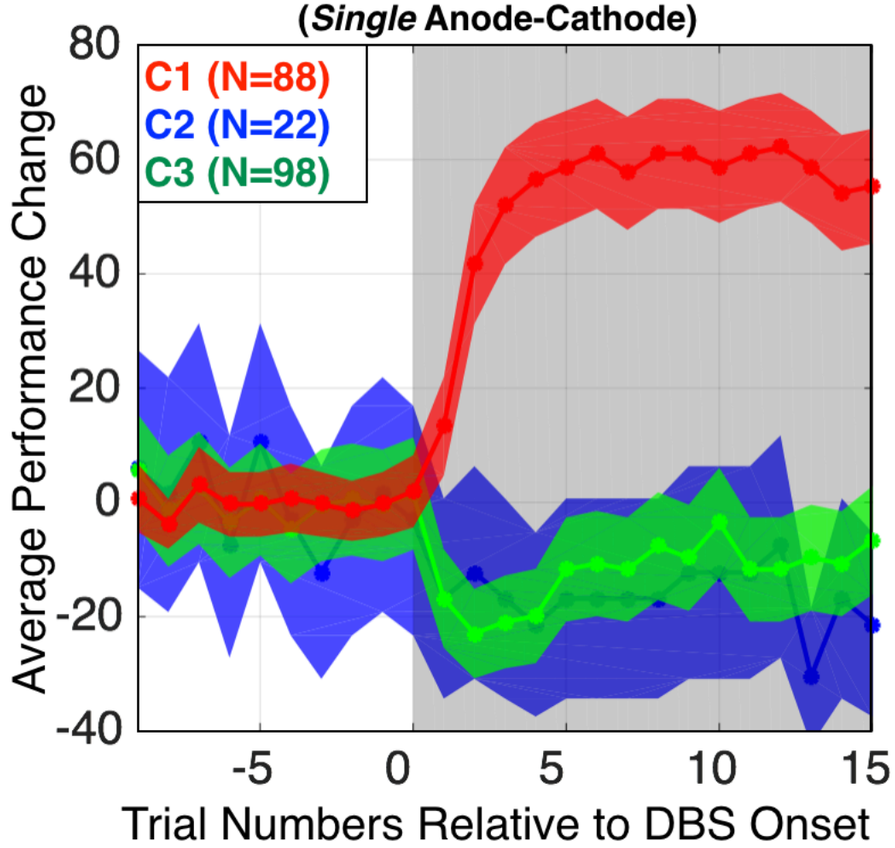

C

Frontal-Striatal Activation

(*Single* Anode-Cathode)

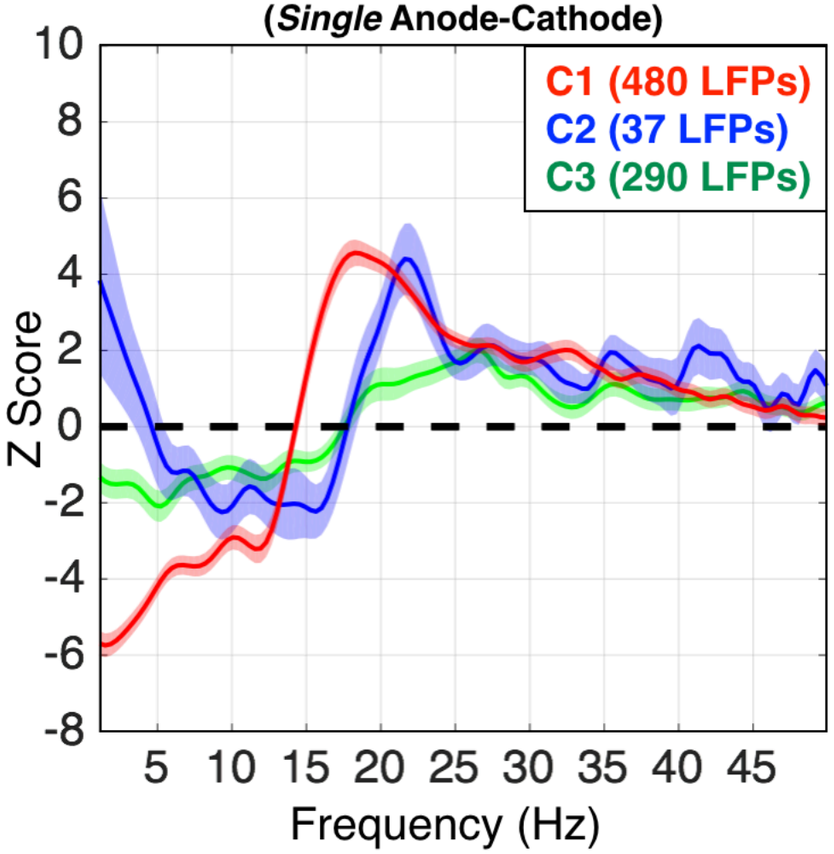

D

(*Dual* Anode-Cathode)

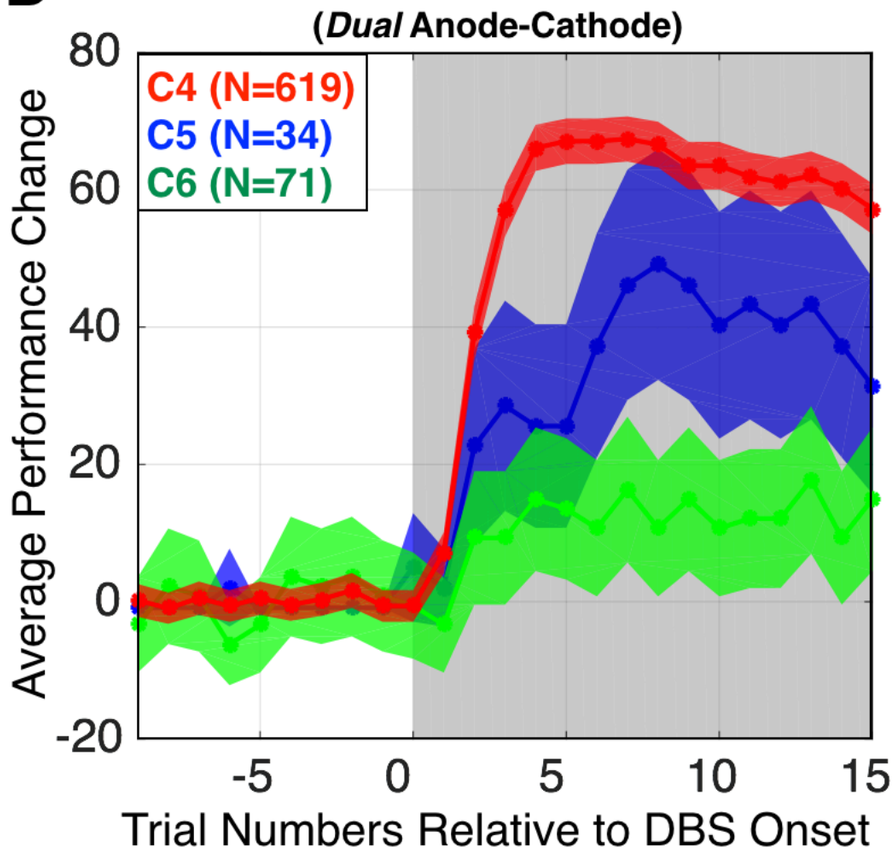

E

(*Dual* Anode-Cathode)

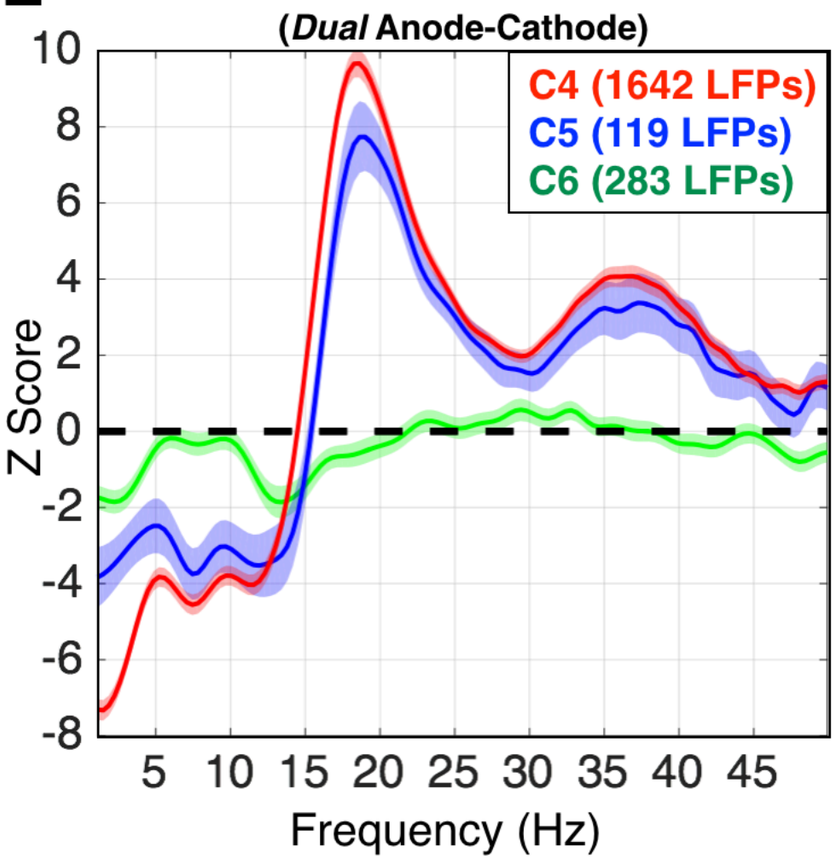

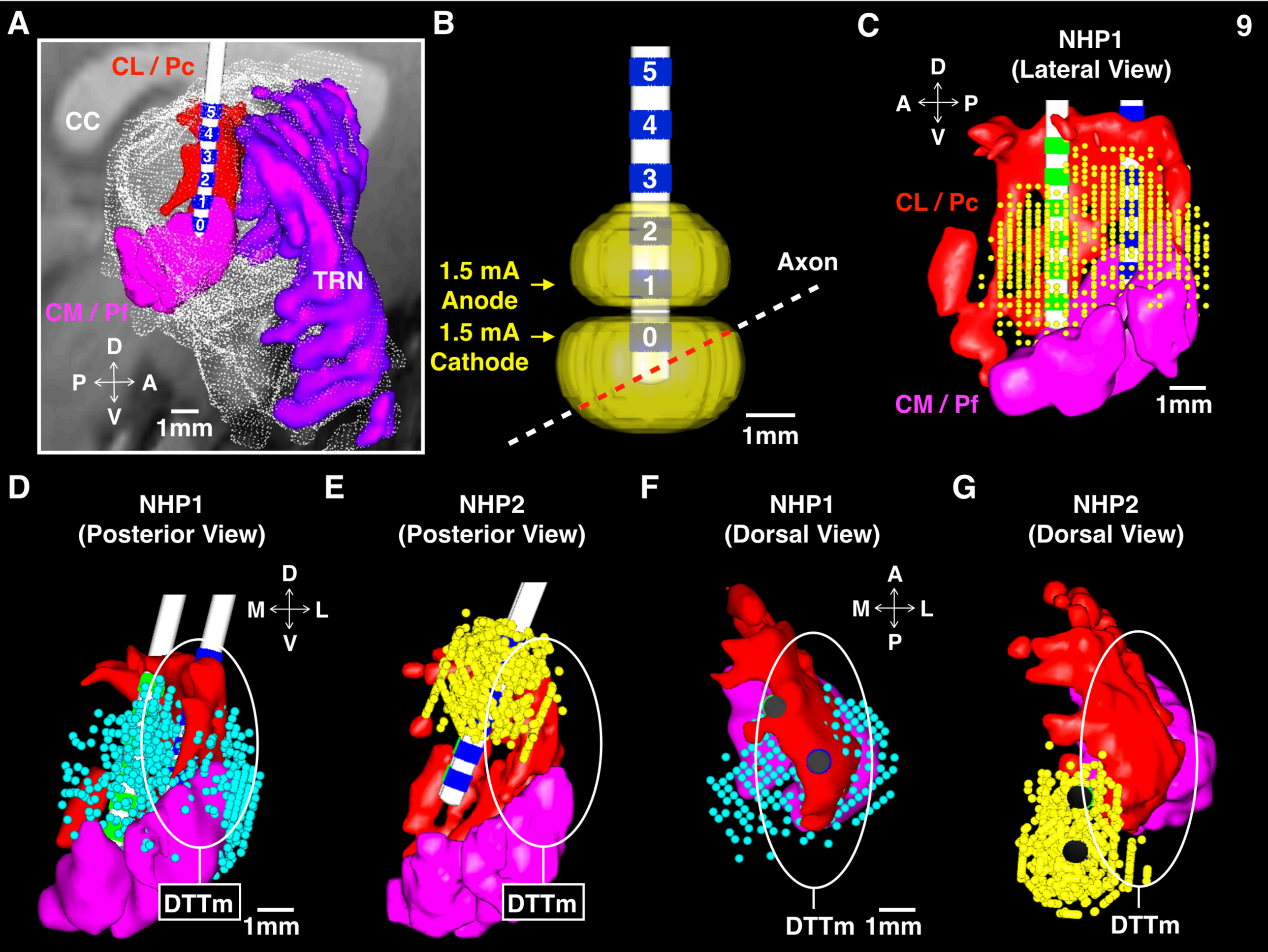
A
CL / Pc
CC
5
4
3
2
1
0
TRN
CM / Pf
D
P
A
V
1mm
B
5
4
3
2
1
0
1.5 mA
Anode
1.5 mA
Cathode
Axon
1mm
C
NHP1
(Lateral View)
D
A
P
V
CL / Pc
CM / Pf
1mm
D
NHP1
(Posterior View)
D
M
L
V
DTTm
1mm
E
NHP2
(Posterior View)
DTTm
F
NHP1
(Dorsal View)
A
M
L
P
DTTm
1mm
G
NHP2
(Dorsal View)
DTTm

A

Frontostriatal 'activation' with fsCT-DBS

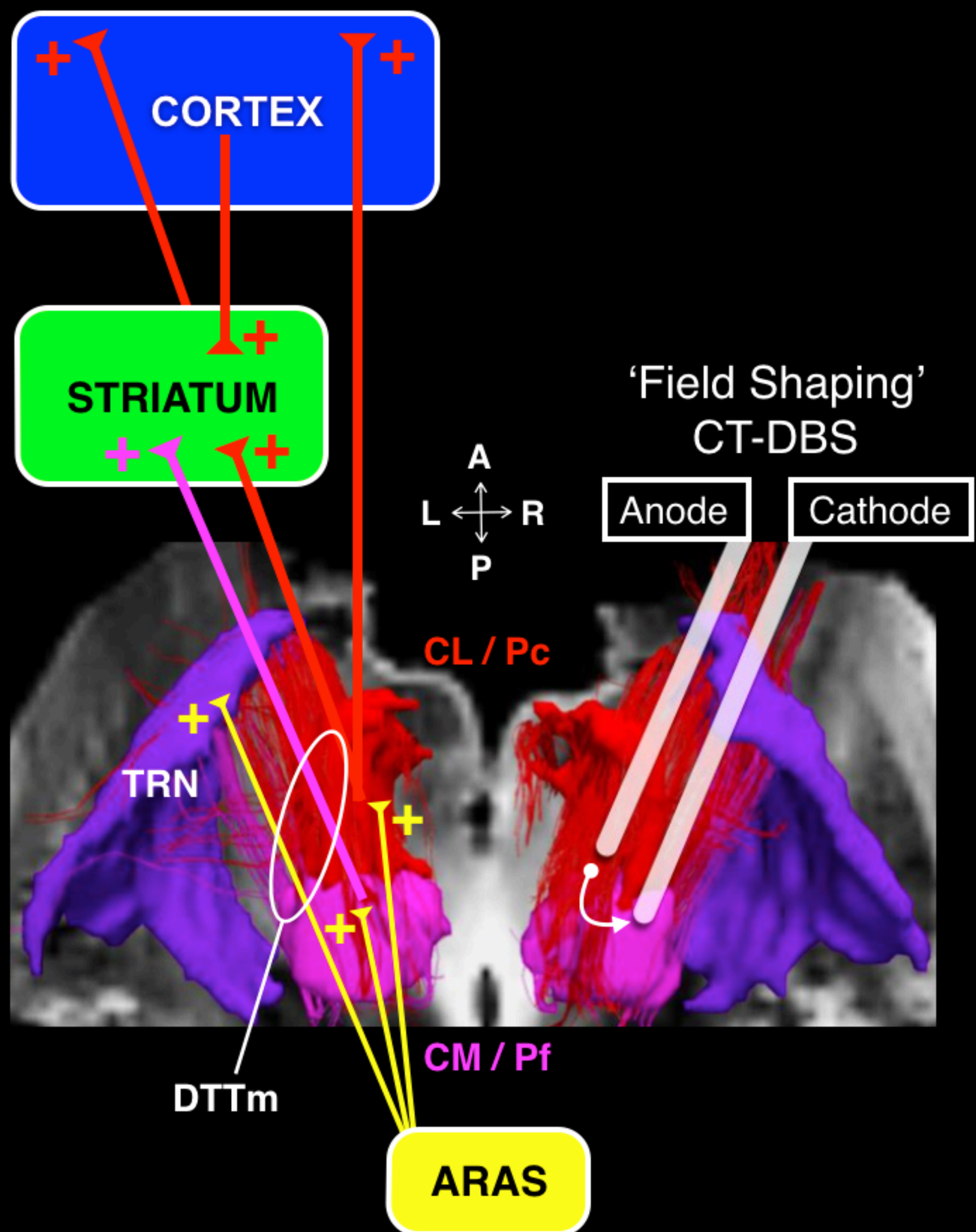

B

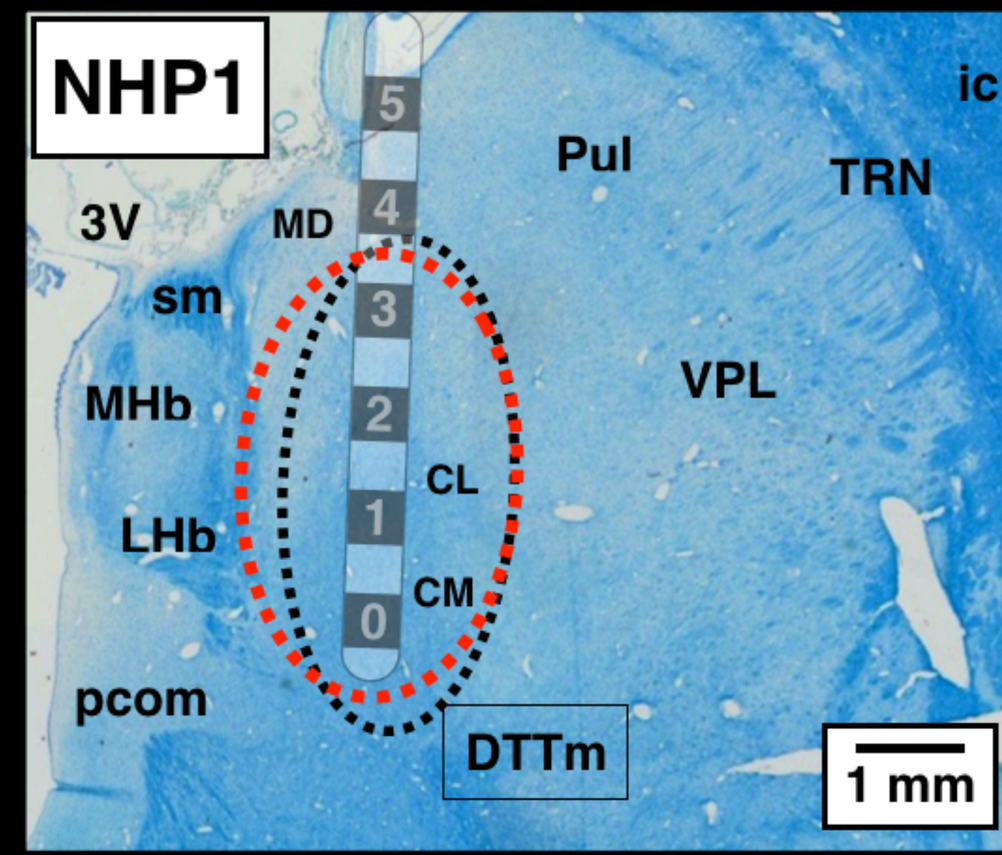

C